

Defect Engineering of Photocatalysts for Solar Energy Conversion

Lei Ran, Jungang Hou,* Shuyan Cao, Zhuwei Li, Yanting Zhang, Yunzhen Wu, Bo Zhang, Panlong Zhai, and Licheng Sun*

Solar energy conversion is one of the most versatile approaches for sustainable energy demands. The fundamental limitations for photocatalysis remain light absorption, charge separation, and photocatalytic (PC) performance of the catalysts. For the past few decades, defect engineering has been proven to be a promising solution for converting solar energy to chemical energy. In this regard, the recent progress of defect engineering toward solar energy conversion is summarized. Beginning with defects classification, the definition of various defects, synthesized strategies, and characterization techniques of controllable material defects are presented. The role of defect engineering on solar energy conversion is developed, extending light absorption, promoting charge separation, and facilitating stable PC reaction. The achievement of the defective photocatalysts is discussed toward versatile applications such as solar water splitting, CO₂ reduction, nitrogen fixation, molecular activation, pollutants degradation, and solar cells. Finally, this Review, with regards to defect engineering, ends with the future opportunities and challenges for this exciting and emerging area for solar energy conversion.

1. Introduction

With increasing energy demands, environmental concerns, and even climate change issues, exploiting renewable energy sources and developing low-cost energy utilization routes are of great significance for our modern society.^[1] Among various renewable energy sources, solar energy is regarded as promising one meeting the imperative societal demand for sustainable clean energy due to its inexhaustibility, universality, high capacity, and environmental friendliness. For example, photocatalytic (PC) or photoelectrochemical (PEC) reactions have been significantly

concerned.^[2,3] With the development of PC technology, it is gradually extending the perspective field, such as solar CO₂ reduction and N₂ fixation and solar cell, and so on.^[4–7]

Generally, solar energy conversion system always involves three different steps about charge generation, charge separation, and catalytic reactions.^[8,9] A substantial proportion of the efforts were conducted to exploit the promising semiconductors.^[10–16] However, the low efficiency is mainly ascribed to wide bandgap, poor charge transfer, and poor stability. With regard to the aforementioned issues, tremendous strategies have been developed to address these drawbacks. To increase surface areas and active sites for catalytic reaction, morphology engineering with hierarchical nanostructures (such as microspheres, nanowires, nanobowls, nanotubes, nanosheets, and nanoplates) have been explored.^[17–21] To enhance charge separation, heterojunction engineering utilizes different semiconductors with highly matched band alignment.^[22–24]

Alternatively, it is necessary to regulate light absorption, charge separation, and PC performance of the photocatalysts by defect engineering.^[25,26] Generally, the defects are detrimental to PC properties of the photocatalysts due to the charge recombination centers in the defects. Nevertheless, tremendous works confirm the positive roles of the defects in solar energy conversion system.^[5,6] Thus, it is essential to review the accomplishments of various defects upon the design and the PC efficiency of the photocatalysts.

In light of aforementioned background, herein, we have attempted to review the recent achievements in defect engineering for solar energy conversion, as shown in **Figure 1**. Based on the categorization of the defects, we discuss the modulation of light absorption, charge separation, catalytic activities, and stability through defect engineering. Moreover, the breakthrough in controllable strategies of the defects together with characterization techniques is summarized. We highlight various characterization techniques to understand the role of the defects upon the PC performance for solar energy conversion. Finally, we concretely outline the application by defect engineering in solar energy-related fields, including water splitting, CO₂ reduction, nitrogen fixation, molecular activation, pollutants degradation, and solar cells.

Dr. L. Ran, Prof. J. Hou, S. Cao, Z. Li, Y. Zhang, Y. Wu, B. Zhang, P. Zhai, Prof. L. Sun

State Key Laboratory of Fine Chemicals
DUT-KTH Joint Education and Research Center on Molecular Devices
Institute of Energy Science and Technology
Dalian University of Technology (DUT)
Dalian 116024, China
E-mail: jhou@dlut.edu.cn; lichengs@kth.se

Prof. L. Sun
Department of Chemistry
KTH Royal Institute of Technology
Stockholm 10044, Sweden

 The ORCID identification number(s) for the author(s) of this article can be found under <https://doi.org/10.1002/solr.201900487>.

DOI: 10.1002/solr.201900487

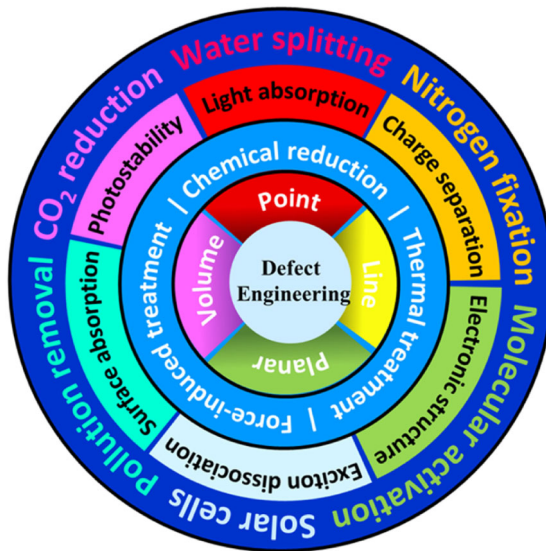


Figure 1. Illustration of defective photocatalysts for solar energy conversion.

2. Classification of Defects

Generally, the defects have been classified according to the atomic structures or the location of the defects in the semiconductor photocatalysts. In principle, as shown in **Figure 2**, all structural irregularities in the photocatalysts can be rationally divided into following four main divisions according to the dimensions: point defects (vacancy),^[27] line defects (edge dislocation and screw dislocation),^[28] planar defects (twin and grain boundary),^[29] and volume defects (void and lattice disorder).^[30]

2.1. Point Defects

With regard to point defects, there are two types of classical point defects including vacancy and dopant. Due to missing atoms, the anion and cation vacancies are vacant positions for the lattice of the photocatalysts. For example, various metal oxides with oxygen vacancies (OVs) including TiO_2 ,^[31] WO_3 ,^[32] Fe_2O_3 ,^[33] BiVO_4 ,^[34] BiO_x ,^[35,36] and carbon vacancies for C_3N_4 ,^[37] nitrogen vacancies for C_3N_4 ,^[38] oxynitrides,^[39] halogens vacancies for $\text{Bi}_7\text{O}_9\text{I}_3$,^[40] and sulfur vacancies for ZnS ,^[41] CdS ,^[42] ZnIn_2S_4 ,^[43] have attracted more attention for solar energy conversion. Apart from the OVs, researchers have developed many photocatalysis with cation vacancies, such as titanium vacancies in TiO_2 ,^[44] stannum vacancies in SnCoFe perovskite hydroxide,^[45] iron vacancies in $\delta\text{-FeOOH}$,^[46] and zinc vacancies in ZnIn_2S_4 .^[47] Typically, self-doped substitution is another way to generate the vacancies in PC materials. For instance, self-doped Ti^{3+} sites can be produced at OV in TiO_2 without any dopants.^[44] Moreover, the multivacancies including different vacancies can also be obtained, such as manganese–cobalt vacancies for $\text{Mn}_{x}\text{Co}_{3-x}\text{O}_4$,^[48] oxygen–zinc vacancies for ZnO ,^[49] and oxygen–titanium vacancies for TiO_2 .^[50] Thus, it is interesting to regulate the formation of the defects in the semiconductor photocatalysts by vacancy creation and self-doping approaches.

Except for vacancy engineering, the component has also been modulated through doping strategy by the introduction of foreign



Lei Ran received her B.S. degree from Sichuan University and her Ph.D. from Shandong University in 2014 and 2019. She is currently a postdoctoral fellow in Professor Jungang Hou's group at the Dalian University of Technology (DUT). Her research interests focus on the controlled synthesis of semiconductors and the applications of photocatalysis and photoelectrocatalysis.



Jungang Hou is currently a full professor at Dalian University of Technology. He received his PhD (2010) from Tianjin University. He joined the faculty of the University of Science and Technology Beijing and was promoted to associate professor in 2013. He worked in Tohoku University as a fellow of Japan Society for the Promotion of Science (JSPS) from 2014 to 2015. His recent research interests focus on the development of photocatalysts and electrocatalysts, PC and electrocatalytic water splitting, CO_2/N_2 conversion to valuable chemicals, and synthesis and applications of nanostructured materials.



Licheng Sun received his PhD in 1990 from the Dalian University of Technology (DUT). He went to Germany as a postdoc at Max-Planck-Institut für Strahlenchemie with Dr. Helmut Görner (1992–1993) and then as an Alexander von Humboldt fellow at Freie Universität Berlin (1993–1995) with Professor Harry Kurreck. He moved to the KTH Royal Institute of Technology, Stockholm, in 1995 and became an assistant professor in 1997, an associate professor in 1999 (Stockholm University), and a full professor in 2004 (KTH). His research interests cover artifacial photosynthesis, molecular catalysts for water oxidation and hydrogen generation, functional devices for total water splitting, and solar cells.

element in the photocatalysts. For doping strategy, foreign atoms as dopant impurities are put into the lattice of the host semiconductor. For instance, nonmetallic element- (C, S, N, H, P, B, F, etc) and metallic element- (Fe, Ni, Sn, and rare-earth metals, etc) doped nanomaterials have been utilized to modulate the band structure and electronic properties of the photocatalysts.^[5,6]

2.2. Line Defects

With regard to line defect, edge dislocation and screw dislocation can be recognized as 1D line defects, such as defective TiO_2 ,^[51]

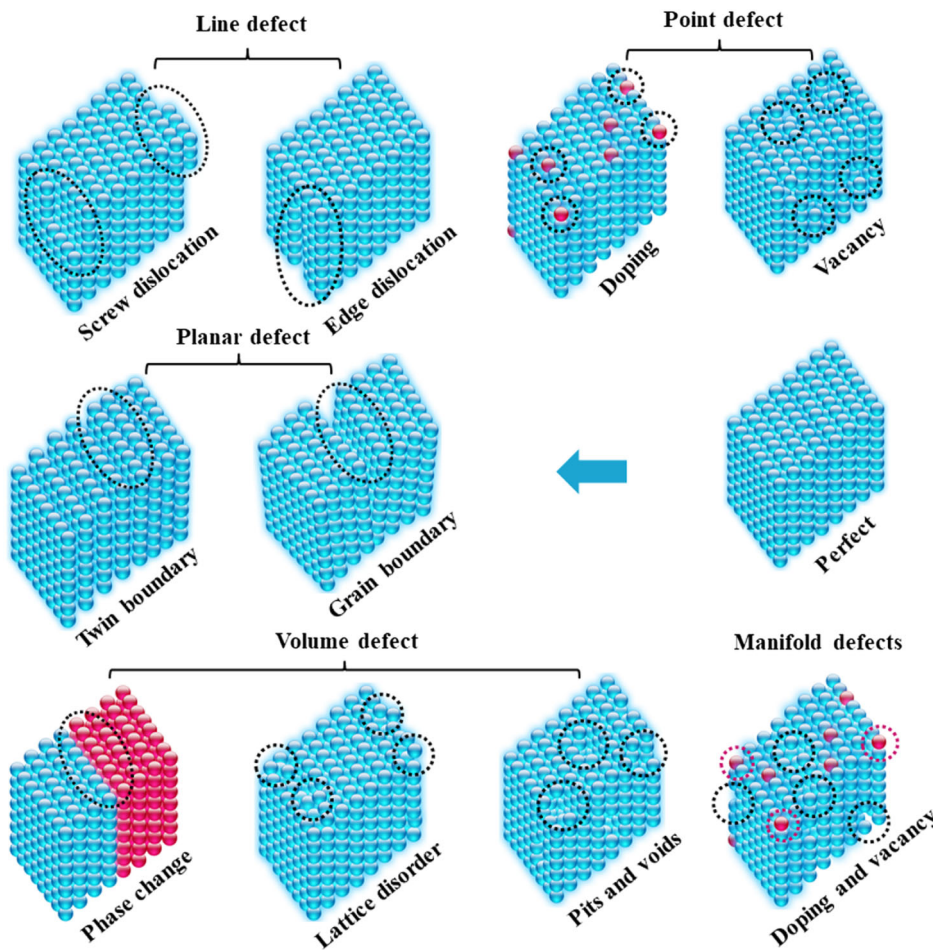


Figure 2. Schematic illustration for various defects with local atomic structures in the photocatalysts.

CdS, and CdSe.^[52] Based on echinoid-shaped and thin nanowire-containing assemblies, the misorientation within the lattice was induced by the edge dislocations in the longitudinal direction of TiO₂ nanobelts. Especially, the excellent PC performance under ultraviolet (UV) illumination is ascribed to the large amount of dislocations in TiO₂ architectures.^[51] Moreover, 1D CdS/CdSe nanowires and nanoribbons were synthesized by a H₂-assisted CVD process, presenting the evidence of the dislocation-driven nanowire growth mechanism. Typically, gold nanoparticles were utilized, providing nucleation sites to initiate the growth of CdS/CdSe nanowires and resulting into the formation of dislocations.^[52] Compared with point defects with the introduction of vacancies and dopants, it is worth mentioning that there is no change upon the components of the photocatalysts.

2.3. Planar Defects

While the planar defects refers to grain boundary and twin boundaries in mixed-phased Bi₂O₃ and Ga₂O₃ with α - β phases^[53] and Cd_{0.5}Zn_{0.5}S.^[29] It is well-known that the heterojunction can optimize charge transfer and separation in photocatalysis. Inspired by this point, it is a great challenge to produce phase junctions for overall water splitting. For example, Ga₂O₃

semiconductors with well-structured α - β phase junctions were fabricated by phase transformation from α -Ga₂O₃ into β -Ga₂O₃ at elevated temperatures, presenting the boundary of α -phase core and β -phase shell and thus resulting into the enhancement of the PC performance for overall water splitting.^[53] Moreover, a twinned Cd_{0.5}Zn_{0.5}S anisotropic nanocrystal as typical twin-induced 1D homojunctions with the alternating zinc-blende and wurtzite segments, presented controllable aspect ratios and a high proportion of long-range-ordered twin planes. Especially, the remarkable PC behavior is ascribed to the efficient separation and the prolonged lifetime of photogenerated charges in the twin-induced homojunctions.^[29] Therefore, there is also no apparent influence upon the stoichiometric compositions of the photocatalysts.

2.4. Volume Defects

For the volume defects, lattice disorders, and voids (or pits) can be regarded to 3D volume defects.^[54] The electronic structures and relative properties of the photocatalysts can be tuned by lattice defects, such as the dislocation and distortion of the lattice and the lattice disorder in HNb₃O₈,^[55] TiO₂,^[56] and Ti_xAg_{1-x}O₂.^[57] For instance, an ultrathin “biphasic”

ordered-disordered D-HNb₃O₈ junction featured the strong visible-near infra red (NIR) light absorption from 250 to 2500 nm and high photoredox capability due to the *in situ* synthetically immobilized lattice distortion of monolayer nanosheets.^[55] Thus, the generation of volume defects by disorder engineering is proven as an avenue toward wide-spectrum photocatalysts.

In typical circumstances, manifold defects have been appeared in various semiconductors. For example, OVs confined in black TiO₂ were produced through hydrogen treatment, corresponding the existence of hydrogen dopants.^[58] Meanwhile, OVs confined in Bi₂WO₆ nanosheets with the existence of Nb⁵⁺ dopants were produced through the partial substitution of W⁶⁺ ions in Bi₂WO₆ nanosheets by Nb⁵⁺ ions, improving the light absorption and charge separation.^[59] According to the locations of the defects in different photocatalysts, the defects can be divided into bulk defects, surface defects, interfacial defects, respectively. Typically, Xiong et al. presented the relationship of two classifications of the defects in the photocatalysts.^[4] On the basis of aforementioned classifications, it is essential to understand the definition of various defects and the relationship between the types of the defects and PC properties.

3. Strategies for Defects Generation

Considering the positive effect of defect introduction into the semiconductors for solar energy conversion, it is imperative to summarize the promising strategies, such as chemical reduction, thermal reduction, and force-induced reduction toward the generation of controllable defects, understanding the process of the defect formation and the relative mechanism in the photocatalysis.

3.1. Chemical Reduction

To introduce the defects into the semiconductors, chemical reduction approaches such as thermal treatment at reducing atmosphere, chemical reduction by reducing agents, and flame reduction are regarded as the promising strategies to create the surface defects into various photocatalysts. Using the reducing atmosphere, such as H₂, CO, NH₃, and H₂S, various defects can be generated in the photocatalysts.^[60–69] For instance, CO and H₂ atmosphere were used to reduce TiO₂, presenting the OVs and disorder layers in H-TiO₂ and CO-TiO₂.^[60] Using thermal treatment, carbon vacancies confined in porous g-C₃N₄ nanosheets with sulfur-doping were collected in NH₃ atmosphere.^[61] Typically, through two-step thermal treatment, N vacancy and phosphorus confined in g-C₃N₄ under H₂ atmosphere was synthesized for PC nitrogen fixation.^[62] Therefore, the thermal treatment at reducing atmosphere is a facile and versatile way to generate diversified defects and even manifold defects in the target photocatalysts.

Using reducing reagents like NaBH₄, KBH₄, CaH₂, N₂H₄, NaH, Zn powder, Al powder, or reducing solvents like ethanol, methanol, and ethylene glycol, the defects can be introduced into the semiconductors through *in situ* chemical reduction. For example, Li et al. utilized a chemical reduction process to prepare the defective Zn₂In₂S₅ nanosheets using reductive ethanol solvents, resulting into the enhancement of solar-driven water splitting (Figure 3a).^[63] The improvement of light absorption and

conductivity is ascribed to the synthesis of vanadium vacancies-confined in o-BiVO₄ layers by this chemical reduction route (Figure 3d).^[64] Nitrogen vacancies confined in carbon nitride was produced through the treatment of thermal polymerization by the assistance of N₂H₄·H₂O, improving the PC performance of solar hydrogen generation.^[65] The OVs and copper dopant co-confined in TiO₂ nanosheets were produced by ethanol reduction strategy (Figure 3b), enhancing the activity of N₂ photofixation due to the introduction of the strain induced by oxygen-vacancies and Jahn-Teller effect.^[66] In comparison with the treatment of reducing atmosphere and reducing agents, it is so fast to generate the vacancies by flame reduction. For instance, a number of Fe₂O₃, ZnO, and BiVO₄ arrays were synthesized through flame reduction treatment, facilitating the improvement of PEC performance of these arrays.^[67,68] The cavities and OVs confined in nickel-iron layered double hydroxides (LDHs) were synthesized by a fast flame-treated approach (Figure 3c), improving OER activities.^[69] Thus, a series of chemical reduction techniques provide the typical features of the defective photocatalysts by defects engineering.

3.2. Thermal Treatment

Generally, the defects could be introduced into the photocatalysts by conventional thermal annealing treatment due to the accelerated escape of the atoms.^[70–76] For instance, the OVs confined in WO₃ nanosheets were prepared using the alcoothermal treatment and subsequent vacuum/hydrogen post-treatment, enhancing PC performance due to the multichannel harvesting of solar light (Figure 4c).^[70] Yang et al. developed a versatile approach to produce melon polymer matrix with carbon vacancies using of steam-etching route in oxygen-deficient environment. Especially, the enhanced PC activity toward solar-driven conversion of CO₂ to CO is ascribed to the generation of active sites and the long charge lifetime.^[71] Apart from oxygen-deficient environment, the high temperature treatment at air atmosphere is also an efficient solution to construct defect-rich semiconductors. For instance, Wang and coworkers developed silicon-based photocathodes with graded-oxygen-defects-confined-in TiO₂ protective layer under the high temperature treatment in air and under vacuum, achieving the excellent current density and outstanding durability in alkaline media (Figure 4a,b).^[72] Jiang and coworkers introduced nitrogen defects and oxygen dopants into porous g-C₃N₄ nanosheets through this facile thermal calcination in air.^[73] Thus, the defects can be produced in the semiconductors by high temperature treatment in oxygen-deficient environment and air atmosphere. Moreover, the vacancies confined in CeO₂, In₂O₃, WO₃, and Co₃O₄ nanosheets can also be produced through phase transformation strategy using CeCO₃OH, In(OH)₃, WO₃·2H₂O, and CoO nanosheets, as the precursors.^[54,74–76] Thus, the defects are also generated during phase transformation process.

Recently, hydrothermal and solvothermal methods as well as ion-exchange process have been developed to synthesize defect-contained photocatalysts with the advantages of the facile set up, simple operations and low cost as well as desirable targets.^[77–79] For example, the defective g-C₃N₄ was produced via hydrothermal method (Figure 5c).^[77] By virtue of the universality of ion exchange route, the dopants can also be introduced to the nonlayered

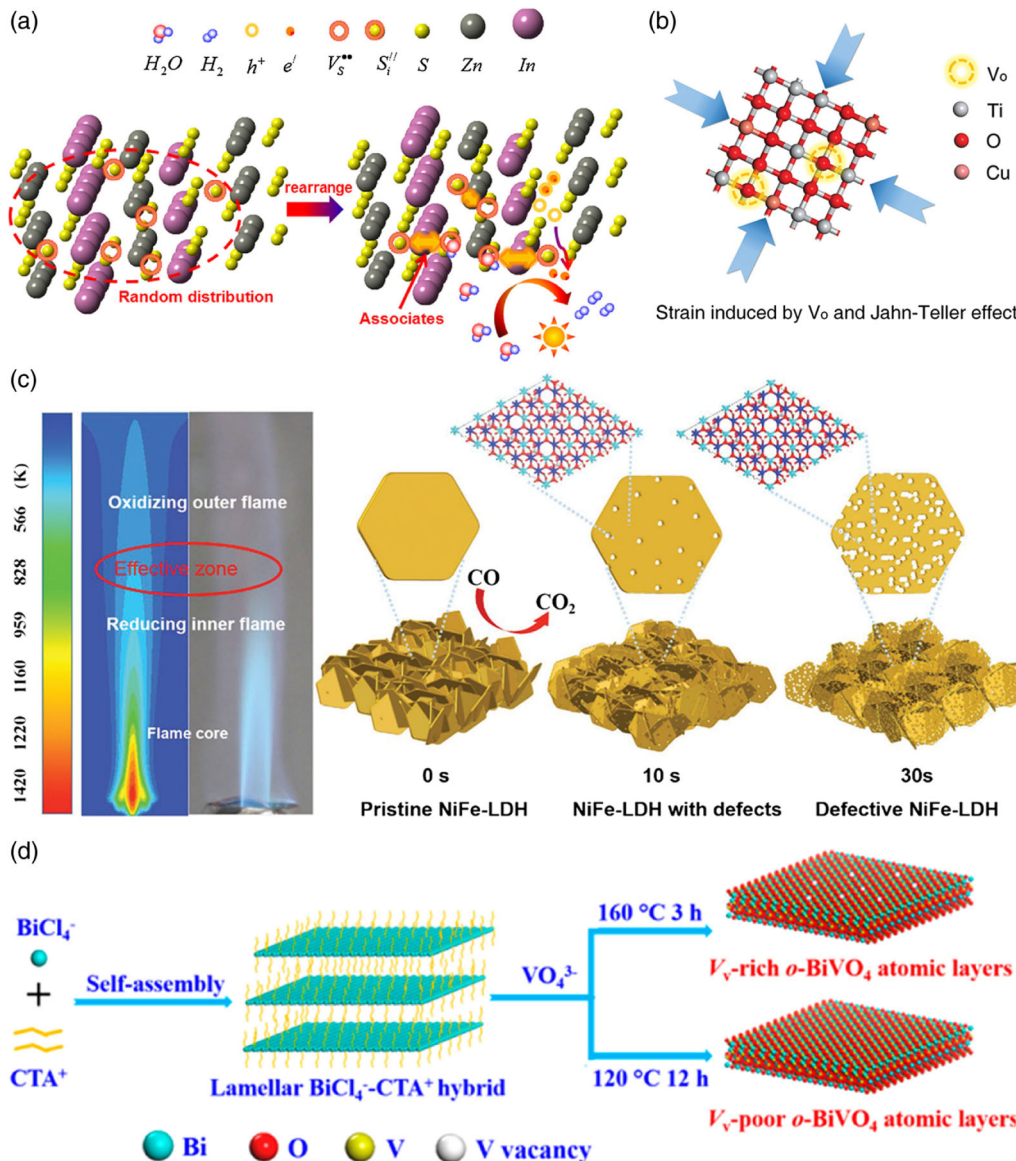


Figure 3. a) Scheme of defective $Zn_2In_2S_5$ nanosheets. Reproduced with permission.^[63] Copyright 2019, Elsevier Ltd. b) Structural model of defective TiO_2 nanosheets. Reproduced with permission.^[66] Copyright 2019, Wiley-VCH. c) Schematic synthesis of defective NiFe-LDH. Reproduced with permission.^[69] Copyright 2018, Wiley-VCH. d) Schematic synthesis of V_v -rich and V_v -poor α - $BiVO_4$. Reproduced with permission.^[64] Copyright 2019, Wiley-VCH.

photocatalysts through ion exchange as described earlier, for instance, Mn^{2+} ions were imported into Cu_7S_4 phase to partially substitute Cu^+ ions using cation-exchange process, dramatically improving PC performance of hydrogen generation (Figure 5a).^[78] Defective HNb_3O_8 (D- HNb_3O_8) monolayers due to ordered-disordered junction structure were fabricated by a cation-exchange-assisted exfoliation strategy. Typically, the harvesting range from 250 to 2500 nm toward full spectrum absorption of as-synthesized D- HNb_3O_8 was realized for excellent PC hydrogen evolution (Figure 5b).^[55] Bi_2MoO_6 nanosheets were synthesized by template-directed ion exchange approach, modulating electronic structure, and charge separation of defective Bi_2MoO_6 .^[79] Therefore, these thermal treatment strategies are promising approaches for the design and the fabrication of the defective photocatalysts.

3.3. Force-Induced Method

Based on the aforementioned defects generation strategies, several force-induced approaches, such as plasma etching, liquid-ammonia-assisted lithiation strategy, UV irradiation, and ball milling have been developed for the synthesis of the defective photocatalysts in the field of solar energy conversion.

The defects could be introduced into the semiconductors by plasma etching as a promising strategy.^[80–86] For example, as-synthesized $In_{2-x}O_3/In_2S_3$ layers with OVs were fabricated by plasma treatment (Figure 6). According to the analysis of theory calculations and experimental observations, as-obtained $In_{2-x}O_3/In_2S_3$ layers showed the excellent activities of broadbandlight PEC water splitting (Figure 6).^[80]

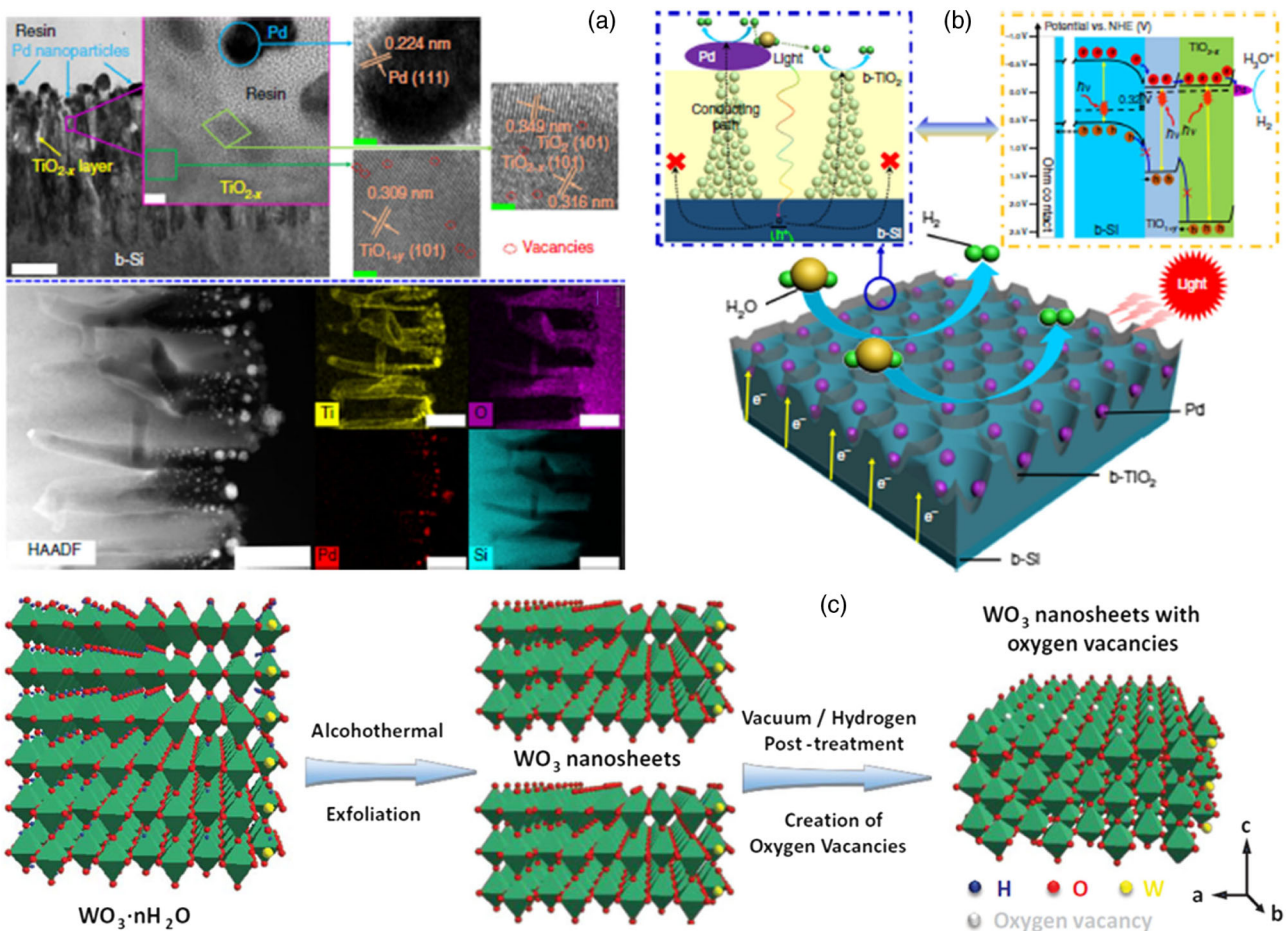


Figure 4. a,b) Microstructure and schematic synthesis of defective TiO₂ protected silicon-based photocathode. Reproduced with permission.^[72] Copyright 2018, Nature Publishing Group. c) Schematic synthesis of defective tungsten oxide. Reproduced with permission.^[70] Copyright 2015, Wiley-VCH.

Oxygen-vacancies-confined in TiO₂ crystals were produced through Ar plasma etching strategy, enhancing charge separation and promoting PC performance of water splitting.^[81] Moreover, the defects could also be introduced into the nanomaterials through a liquid-ammonia-assisted lithiation strategy.^[82–86] For example, sulfur-vacancies-confined in ZnIn₂S₄ (V_s-ZnIn₂S₄) nanosheets were fabricated through a lithiation-chemistry approach (Figure 7), manipulating the electronic structure and the PC performance of defective ZnIn₂S₄ nanosheets. To promote the charge separation of ZnIn₂S₄, the high PC hydrogen generation rates, 6.884 and 11.9 mmol g⁻¹ h⁻¹, were achieved using as-synthesized hybrids of MoS₂ quantum dots/V_s-ZnIn₂S₄ and Z-scheme NiS/WO₃/V_s-ZnIn₂S₄ heterostructures due to the introduction of the defect and the construction of the heterostructure.^[82,83] Meanwhile, hydrogenated ZnIn₂S₄ with the defects using UV irradiation presented the wide spectrum responsive photocatalysis.^[84] Surface OVs on TiO₂ photoelectrodes using atomic layer deposition promoted the performance of PEC N₂ fixation to ammonia.^[85] Compared with aforementioned process, ball-milling is regarded as a facile strategy to generate the defects in the semiconductors. For instance, OVs and bismuth vacancies

confined in BiPO₄ was produced by the regulation of the power and time of ball-milling process, promoting the PC property.^[86] Thus, the synthesized strategy plays a pivot role upon the PC application of the defective photocatalysts.

4. Understanding the Role of Defect Engineering on Solar Energy Conversion

As the positive influence of the defects upon the light absorption, charge separation, and catalytic activities as well as defect visualization and quantification has been greatly investigated,^[87–100] it is essential to understand the roles of the defects on solar energy conversion by the photocatalysts.

4.1. The Modulation of Light Absorption by Defect Engineering

Generally, the light absorption range is depending on the bandgap structures of the photocatalysts. In particular, the range of light absorption can be modulated by the introduction of the defects.^[87–91] For instance, Liu et al. reported a red anatase TiO₂

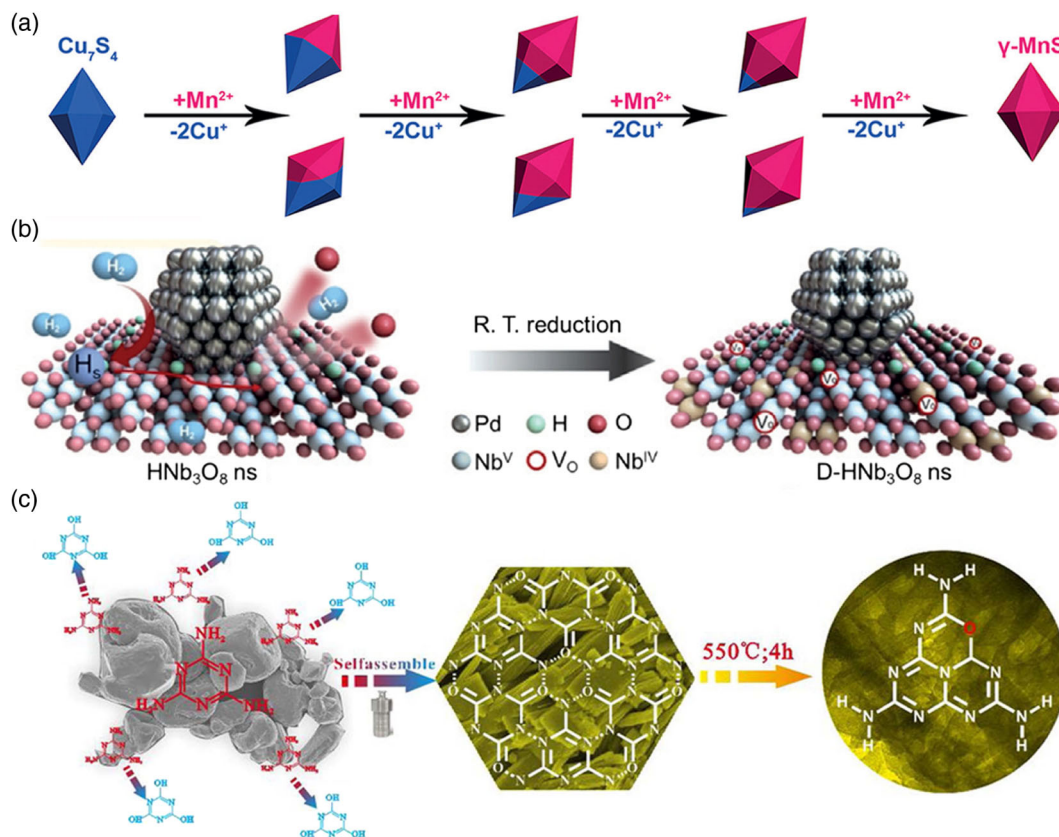


Figure 5. a) Schematic synthesis of γ -MnS/Cu₇S₄. Reproduced with permission.^[78] Copyright 2017, Wiley-VCH. b) Schematic synthesis of defective HNb₃O₈. Reproduced with permission.^[55] Copyright 2019, Wiley-VCH. c) Schematic synthesis of defective g-C₃N₄. Reproduced with permission.^[77] Copyright 2018, Elsevier Ltd.

with inner defects (Figure 8a), tuning bandgap range from 3.22 to 1.94 eV and thus extending the light absorption of TiO₂.^[87] Compared with common oxygen-deficient TiO₂, Liu and co-workers developed a facile strategy to produce red anatase TiO₂ with atomic hydrogen-mediated OVs (Figure 8b), prolonging the light absorption range from 400 to 712 nm and regulating the electronic structure of TiO₂.^[88] At the same time, B/N codoped TiO₂ microspheres with intrinsic defects presented the light absorption edge up to 680 nm (Figure 8c).^[89] Zhang and coworkers developed alkali-assisted process to synthesize nitrogen defective g-C₃N₄ using KOH, NaOH and Ba(OH)₂ as alkali compounds (Figure 8d), controlling the bandgap range from 2.68 to 2.36 eV.^[90] Shen and coworkers reported defective g-C₃N₄ (Figure 8e,f), regulating the bandgap range from 2.66 to 1.4 eV and achieving the excellent PC oxygen generation rate.^[91] Thus, the modulation of the defects is an effective strategy to regulate light absorption and bandgap structures of the photocatalysts.

4.2. The Modulation of Charge Transfer and Separation by Defect Engineering

Apart from the light absorption, the charge separation has been optimized in the defective photocatalysts, highlighting the pivot role of the defects in the photocatalysis.^[92–96] For example,

the PEC performance of hydrogen evolution has been improved due to the optimization of charge transport and surface area using p-type ZrO₂ nanoplates coupled ZrO₂ nanowire photocathode with OVs through hydrofluoric acid treatment (Figure 9a).^[92] 0D/2D heterostructures were synthesized by g-C₃N₄ nanosheets decorated with OV-rich TiO₂ quantum dots, reaching an excellent CO generation rate, appropriately five times of g-C₃N₄.^[93] Wang et al. reported Nb-doped NiO_x/Ni/black-Si photoanodes with OVs, achieving the high PEC performance due to the efficient charge separation by the introduction of the defects (Figure 9b).^[94] CdS/ZnS composites with Z-scheme mechanism were produced using Na₂SO₃ and Na₂S (Figure 9c), presenting the high PC hydrogen evolution rate due to the efficient charge separation.^[95] Moreover, the defective g-C₃N₄ with the light absorption range from 2.75 to 2.00 eV endowed the improved PC hydrogen generation performance due to the generation of p–n homojunction,^[96] facilitating the effective charge separation in the photocatalysts.

4.3. The Modulation of Surface PC Reactions by Defect Engineering

After the regulation of light absorption and charge separation, there is a main task to promote the surface PC reactions by the defects.^[97–100] For example, compared with BiOCl (010)

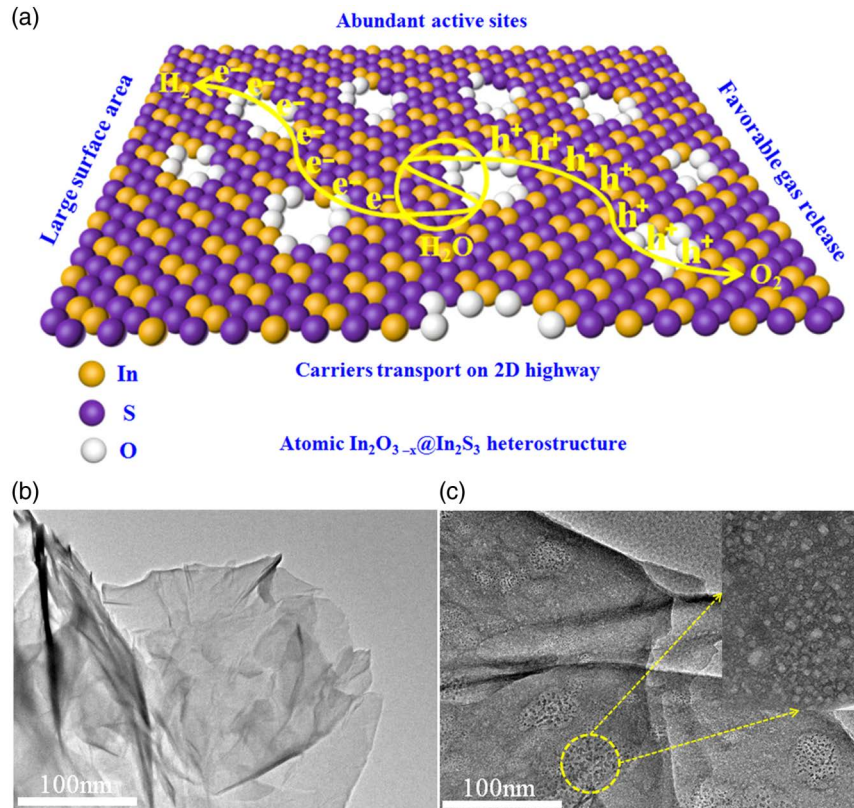


Figure 6. a) Scheme and b,c) TEM images of In_2S_3 and defective $\text{In}_2\text{O}_{3-x}/\text{In}_2\text{S}_3$ layers. Reproduced with permission.^[184] Copyright 2018, Wiley-VCH.

surface, OVs confined in BiOCl (010) surface presented the excellent activity of the photo-oxidation due to the activation of adsorbed water by OVs.^[97] The superior PC performance toward the conversion of CO_2 to hydrocarbons was achieved using carbon-doped SnS_2 ($\text{SnS}_2\text{-C}$) catalysts due to the formation of the microstrain in SnS_2 lattice by carbon doping strategy.^[98] As-synthesized visible-light-driven Bi metal@defective $\text{Bi}_2\text{O}_2\text{SiO}_3$ photocatalysts showed the PC removal of NO due to the effective regulation of light absorption and charge separation by the defects.^[99] Hydrogenated titania with doped hydrogen and OVs (H-TiO_{2-x}) achieved the excellent PC rate of the conversion from CO_2 to CH_4 and superior selectivity due to the enhanced adsorption and chemical activation of CO_2 molecule (Figure 10).^[100]

Based on aforementioned analysis, the main roles of the defects in the photocatalysis are shown in Table 1. It is worth mentioning that other roles of the defects have also been attracted upon the optimization of the PC performance. For instance, the effective exciton dissociation into free charges due to the electron harvesting behavior was observed by order-disorder heptazine-based melon through defects engineering.^[5d] Meanwhile, the exciton dissociation into charge carriers were also conducted using OVs confined in BiOBr , which is ascribed to the distorted localization of band-edge states.^[5e] Defect-mediated Z-scheme $\text{BiO}_{2-x}/\text{Bi}_2\text{O}_{2.75}$ heterojunction played an indispensable role in promoting exciton dissociation, presenting excellent PC activity over the full solar spectrum from UV to NIR light due to the formation of the built-in electric field induced by

Bi and O defects and Z-scheme PC mechanism.^[5f] Moreover, the selective growth of crystal facets on the photocatalysts could be regulated by defects engineering,^[6c,d] providing a promising way to mediate the transfer and separation of photogenerated electrons and holes and accelerate the PC performance due to the facet-dependent band structure in the photocatalysts. Thus, there is a challenge to explore the versatile roles of the defects, promoting the catalytic performance of the photocatalysts.

5. Characterization Techniques of the Defects

As numerous achievements have been obtained upon the modulation of light absorption, charge separation, and PC reactions by defects engineering, it is necessary to evaluate the atomic structures of the defects and determine the relationship between the structure and catalytic activities by characterization techniques.^[101–115]

5.1. Electron Microscopic Techniques

Among various characterization techniques, the most direct way is electron microscopic technique, capturing the defects in the photocatalysts.^[101–106] For instance, a great deal of pits were observed on ZnO nanorods by scanning electron microscope (SEM) and transmission electron microscope (TEM).^[101] TEM image of $\text{g-C}_3\text{N}_4$ nanosheets presented the feature of

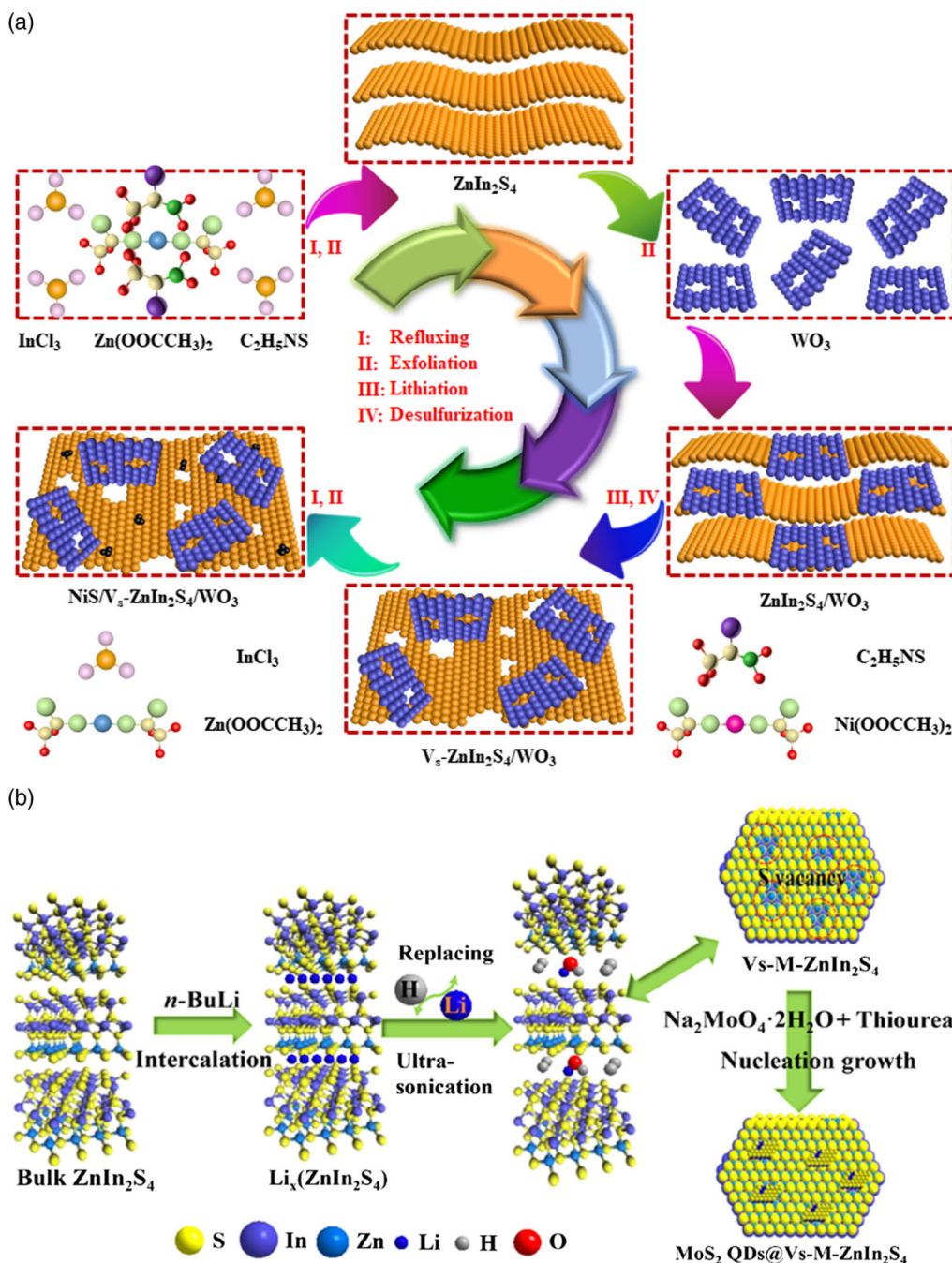


Figure 7. a) Schematic synthesis of $\text{NiS}/\text{WO}_3/\text{V}_5\text{-ZnIn}_2\text{S}_4$ heterostructures. Reproduced with permission.^[82] Copyright 2019, Elsevier Ltd. b) Schematic synthesis of $\text{MoS}_2\text{ QDs}@\text{Vs-M-ZnIn}_2\text{S}_4$ heterostructures. Reproduced with permission.^[83] Copyright 2018, American Chemical Society.

macropores and substantial of mesopores in g-C₃N₄ layer (**Figure 11a**).^[102] To check the details, the edge dislocation can be obviously observed in high-resolution TEM (HRTEM) image of TiO₂ nanowires, indicating the formation of a massive of dislocations.^[103] TEM and high-resolution TEM images of Cu/Cu₂O interface indicated the feature of twin boundaries, promoting the stability of Cu₂O.^[104] The grain boundaries of ZnS(ethylenediamine)_{0.5} nanosheets as organic–inorganic

hybrid semiconductors with defect-rich structure were presented, corresponding a lot of dislocation and stacking fault at the boundaries in HRTEM (**Figure 11b**).^[105] The obvious pores and sulfur vacancies were confirmed by false-color image and HRTEM image of sulfur vacancies confined in ZnIn₂S₄ nanosheets (**Figure 11c,d**).^[82,83] With regard to one-unit-cell ZnIn₂S₄ layers, high-angle annular dark-field scanning transmission electron microscopy (HAADF-STEM) can be utilized for the

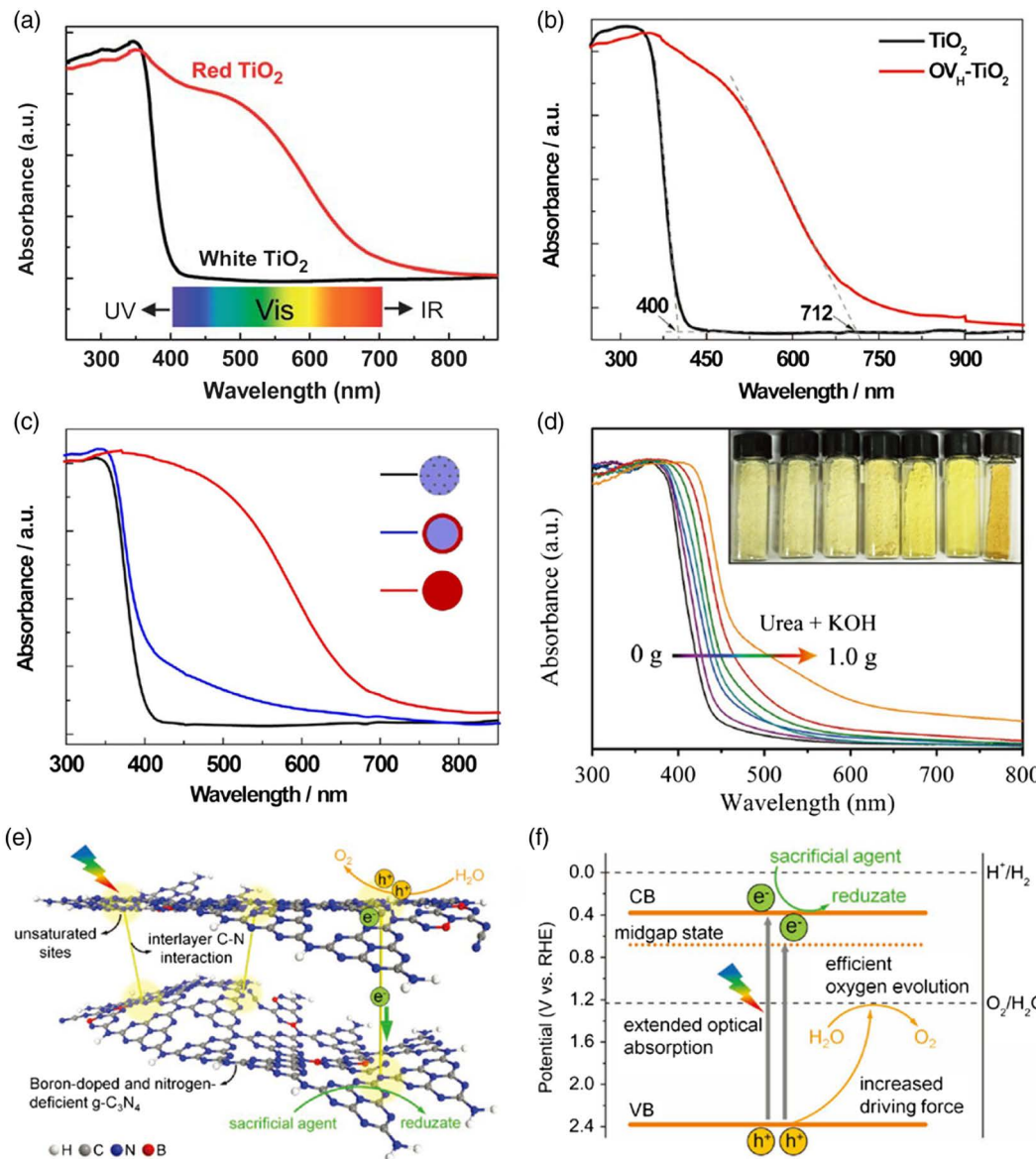


Figure 8. a) UV-vis reflection curves of red TiO_2 . Reproduced with permission.^[87] Copyright 2012, The Royal Society of Chemistry. b) UV-vis reflection curves of oxygen-deficient TiO_2 . Reproduced with permission.^[88] Copyright 2018, Wiley-VCH. c) UV-vis reflection curves of boron and nitrogen in TiO_2 . Reproduced with permission.^[89] Copyright 2019, Wiley-VCH. d) UV-vis reflection curves of defective C_3N_4 . Reproduced with permission.^[90] Copyright 2019, Wiley-VCH. e,f) Charge transfer illustration of defective C_3N_4 . Reproduced with permission.^[91] Copyright 2019, Wiley-VCH.

confirmation of abundant vacancies confined in ZnIn_2S_4 atomic layers.^[47]

To analyze the electronic structure of individual defects, non-contact atomic force microscopy (AFM) and scanning tunneling microscopy (STM) have been utilized to check the influence of the point defect confined in MoSe_2 monolayers upon the electronic structures.^[106] For instance, the hexagonal lattice of bright features was indexed to the outer chalcogen atoms by CO-tip noncontact-AFM, confirming the identification of the lattice sites of MoSe_2 .^[106] Moreover, three bright protrusions on hydroxylated TiO_2 surface were observed by STM,^[109] indicating the visualization of OVs as point defects, adsorbed H_2O (ad- H_2O) molecules,

and OH groups and thus proving a promising way for the visualization investigation of the defects (Figure 11e). Furthermore, energy dispersive X-ray spectroscopy and inductively coupled plasma atomic emission spectroscopy can also be used for the characterization of the defects. Thus, it is still a great challenge to confirm the formation of the defects and analyze the visualization and quantification of the defects by appropriate techniques.

5.2. Spectroscopic Techniques

Apart from microscopic techniques, spectroscopic techniques such as X-ray absorption spectroscopy, in situ electron energy loss

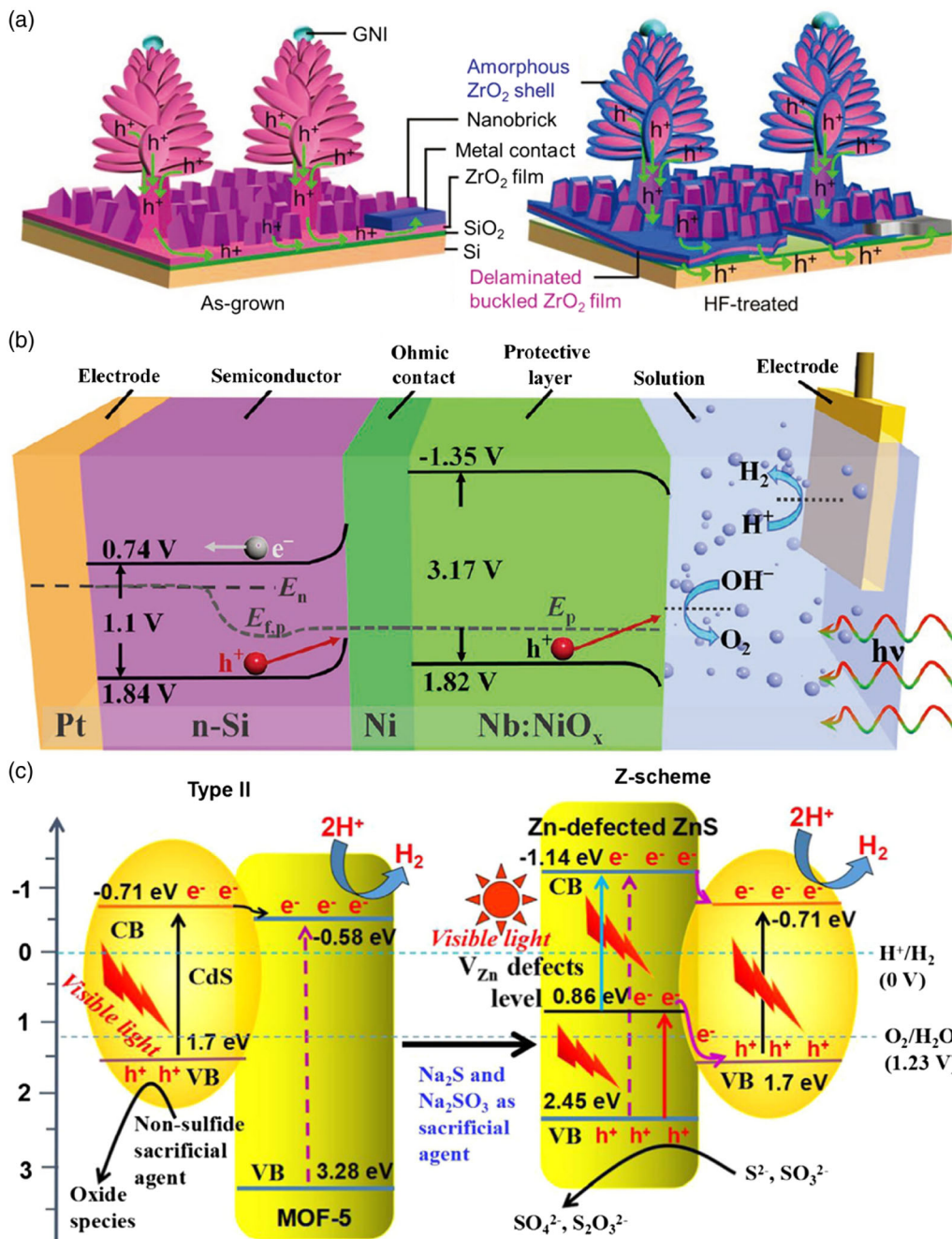


Figure 9. a) Schematic models of defect-rich ZrO_2 hierarchical nanowire film. Reproduced with permission.^[92] Copyright 2017, Wiley-VCH. b) Band structure of NiO_x -based/Ni/black Si photoanode. Reproduced with permission.^[94] Copyright 2018, Wiley-VCH. c) Charge transfer mechanisms over CdS/metal-organic frameworks and Zn-defected CdS/ZnS heterojunctions. Reproduced with permission.^[95] Copyright 2018, Elsevier Ltd.

spectroscopy (EELS), electron paramagnetic resonance (EPR) spectroscopy, positron annihilation spectroscopy, Raman spectroscopy, X-ray photoelectron spectroscopy, and thermogravimetric measurement are indispensable to determine the atomic structures of the defects for the photocatalysts.

Synchrotron radiation X-ray absorption fine structure (XAFS) including extended X-ray absorption fine structure (EXAFS) and X-ray absorption near-edge structure (XANES)

spectroscopy is a widespread way to obtain the insights into the defects of the photocatalysts. For example, NiFe porous monolayer LDH (PM-LDH) with abundant defects was investigated by XAFS spectroscopy, determining the local structure of Ni and Fe cations in PM-LDH.^[107] The combined analysis of XANES and EPR spectra confirmed the formation of OV, nickel vacancy, and iron vacancy in PM-LDH (Figure 12a-d). The two peaks located at 283.8 and 286.6 eV were observed by XANES

Table 1. Summary of typical defective photocatalysts with different defects and synthesis methods as well as characterization techniques.

Material	Roles of defects	Defect types	Mechanism	Application	Refs.
WO ₃	Light absorption modulation	OVs	Formation of new energy levels	PC CO ₂ reduction	[32]
Fe ₂ O ₃	Light absorption modulation	OVs	Narrowed band-gap	PEC water splitting	[33]
C ₃ N ₄	Light absorption modulation	N vacancies	Narrowed band-gap	Photodegradation of rhodamine B	[38]
C ₃ N ₄	Light absorption modulation	N vacancies	Narrowed band-gap	PC water splitting	[90]
C ₃ N ₄	Light absorption modulation	N vacancies B dopants	Narrowed band-gap	PC oxygen evolution	[91]
TiO ₂	Light absorption modulation	B,N dopants	Narrowed band-gap	PC water splitting	[89]
TiO ₂	Light absorption modulation	OVs	Formation of a new subvalence band	PEC water oxidation	[88]
ZnO	Charge transfer and separation modulation	OVs Zn vacancies	p-n homojunction	PEC water splitting	[49]
BiVO ₄	Charge transfer and separation modulation	OVs	Z-scheme recombination	PC oxygen evolution	[34]
Ga ₂ O ₃	Charge transfer and separation modulation	Junctions	α-β phase heterojunction	PC water splitting	[53b]
Bi ₂ O ₃	Charge transfer and separation modulation	Junctions	α-β phase heterojunction	Photodegradation of RhB and MO	[53a]
WO ₃	Charge transfer and separation modulation	OVs	Formation of lower energy levels to trap carriers in Z-scheme	PC CO ₂ reduction	[32]
Bi ₂ WO ₆	Charge transfer and separation modulation	OVs Nb ⁵⁺ dopants	Capturing carriers for surface reactions	Photodegradation of RhB	[59]
Bi ₇ O ₉ I ₃	Charge transfer and separation modulation	I vacancies	Increased carrier density	Peroxymonosulfate activation	[40]
ZnIn ₂ S ₄	Charge transfer and separation modulation	S vacancies	Increased carrier density	PC water splitting	[43]
Cd _{0.5} Zn _{0.5} S	Charge transfer and separation modulation	Twin boundaries	Prolonged lifetime of both photogenerated carries	PC water splitting	[29]
g-C ₃ N ₄	Charge transfer and separation modulation	C vacancies	Increased carrier density	PC CO ₂ Reduction	[37]
ZrO ₂	Charge transfer and separation modulation	OVs	Increased carrier density	PEC hydrogen evolution	[92]
TiO ₂	Charge transfer and separation modulation	OVs	Prolonged lifetime of photo-generated carries	PC CO ₂ reduction	[93]
NiO	Charge transfer and separation modulation	OVs	Capturing carriers for Surface reactions	PEC water oxidation	[94]
ZnS	Charge transfer and separation modulation	Zn vacancies	Formation of lower energy levels to trap carriers in Z-scheme	PC H ₂ evolution	[95]
TiO ₂	Surface reactions modulation	OVsTi ³⁺ dopants	Enhanced adsorption and chemical activation	Peroxymonosulfate activation	[58]
TiO ₂	Surface reactions modulation	OVs H dopants	Enhanced CO ₂ adsorption and chemical activation	PC CO ₂ reduction	[100]
Bi ₁₂ O ₁₇ C ₁₂	Surface reactions modulation	OVs	Enhanced CO ₂ adsorption and chemical activation	PC CO ₂ reduction	[35]
ZnS	Surface reactions modulation	S vacancies	Enhanced CO ₂ adsorption and chemical activation	PC CO ₂ reduction	[41]
BiOCl	Surface reactions modulation	OVs	Enhanced H ₂ O adsorption and chemical activation	PC water oxidation	[97]
SnS ₂ -C	Surface reactions modulation	C dopants	Enhanced CO ₂ adsorption and chemical activation	PC CO ₂ reduction	[98]
Bi ₂ O ₂ SiO ₃	Surface reactions modulation	OVs	Enhanced adsorption and chemical activation	PC NO removal	[99]

spectra of C K-edge and N K-edge for g-C₃N₄ and defective g-C₃N₄ (Figure 12e,f), indicating the presence of nitrogen defects.^[108] Meanwhile, EELS can be used to analyze the distribution of the defects in the photocatalysts. As shown from Ti-L edge spectra, the enhanced concentration of Ti³⁺ ions indicated the increasing content of OVs in reduced TiO₂ crystals.^[109] In particular, the valuable information could be obtained by EPR spectroscopy. Moreover, the enhanced EPR signals of Bi₂WO₆

(BWO) with OVs after the reduction treatment at different temperatures confirmed the existence and the increasing content of OVs in BWO layers (Figure 12g).^[110] The signals of OVs were presented in OVs confined in TiO₂ and Au/TiO₂, indicating the vacancy generation.^[111] To determine the quantities and the types of the defects, positron annihilation spectrometry (PAS) is also regarded as a promising approach. The positron lifetime spectra of defective o-BiVO₄ presented three lifetime

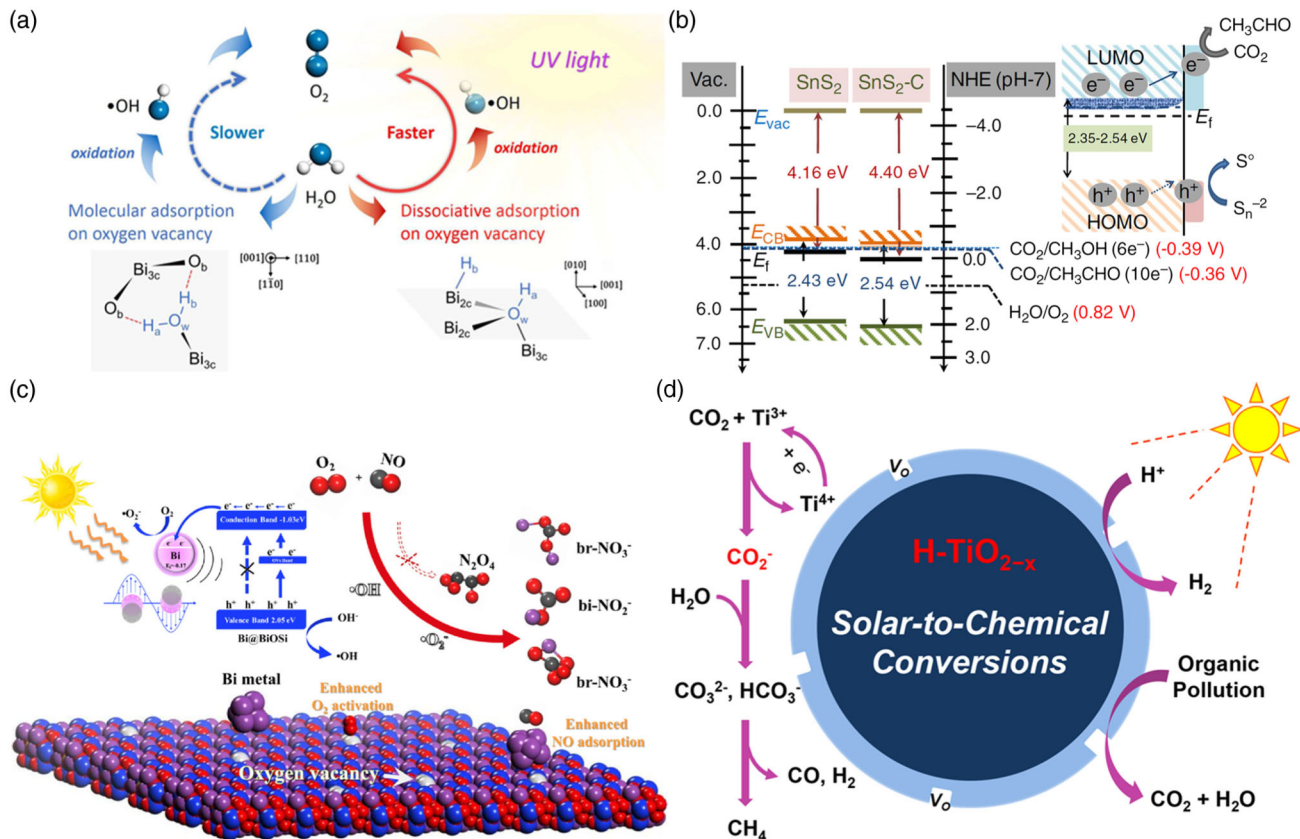


Figure 10. a-d) Scheme of electrons transfer. Reproduced with permission.^[97] Copyright 2016, American Chemical Society. b) Band diagram and mechanism of SnS₂-C and SnS₂. Reproduced with permission.^[98] Copyright 2018, Nature Publishing Group. c) PC processes of defective Bi@Bi₂O₂SiO₃. Reproduced with permission.^[99] Copyright 2019, Elsevier Ltd. d) Reaction pathways of H-TiO_{2-x}. Reproduced with permission.^[100] Copyright 2017, American Chemical Society.

components, demonstrating the existence of vanadium vacancies and the enhanced concentration of vanadium vacancies in o-BiVO₄ layers at high temperature (Figure 12h,i).^[64] OVs confined in BiO_{2-x} monolayers were synthesized by the combined characterization techniques including EPR, positron annihilation lifetime, thermogravimetry, and X-ray photoelectron spectroscopy, indicating the production of BiO_{2-x} monolayers with OVs.^[112] Although the chemical states of the defects under ideal conditions can be conducted by density functional theory calculations, it is still a challenge to explore the direct evidence of dynamic changes of the defects at the atomic level in the photocatalysis. For example, HRTEM images and 2D grazing incidence wide-angle X-ray scattering (2D-GIWAXS) study the surface structure of defective TiO₂ nanocrystals.^[112] Especially, the changes of OVs reacted with H₂O molecules as well as their influences on charge separation capability can be used by a synchronous illumination X-ray photoelectron spectroscopy (SI-XPS) technique, confirming the formation of OVs on TiO₂ surfaces and detecting the changes of the reformed Ti—O bonds and disappeared OVs after the water absorption.^[112] Thus, the combined analysis of theoretical calculations and SI-XPS results confirmed that the formation of OVs in TiO₂ can effectively promote charge separation and PC hydrogen evolution activity.^[112] According to the analysis

of XAFS and EPR spectra, the presence of chlorine vacancy and OV was also confirmed in BiO_{1-x}Cl_{1-y}. Especially, the decrease of the intensity and broadening and the slight shift of Raman spectra also demonstrated the influence of the OVs upon the vibrational features and the structural of BiO_{1-x}Cl_{1-y}.^[113] Based on the exploration of various spectroscopic techniques, it is essential to utilize appropriate techniques, acquiring the precise information of the structures of defects and constructing the relationship between the structure and the performance of the defective photocatalysts.

5.3. Transient Absorption and Fluorescence Spectroscopy

Although the atomic structures of the defects in the photocatalysts can be identified by spectroscopic techniques, it is also essential to utilize transient absorption (TA) and fluorescence techniques such as time-resolved absorption and fluorescence spectroscopy (nanosecond scale) and transient spectroelectrochemical measurements (microsecond scale). For instance, the charge dynamics in real time of defective ZnIn₂S₄ layers was conducted by ultrafast TA spectroscopy (Figure 13a,b), indicating that massive photoexcited electrons were produced owing to high zinc vacancies and the charge separation efficiency

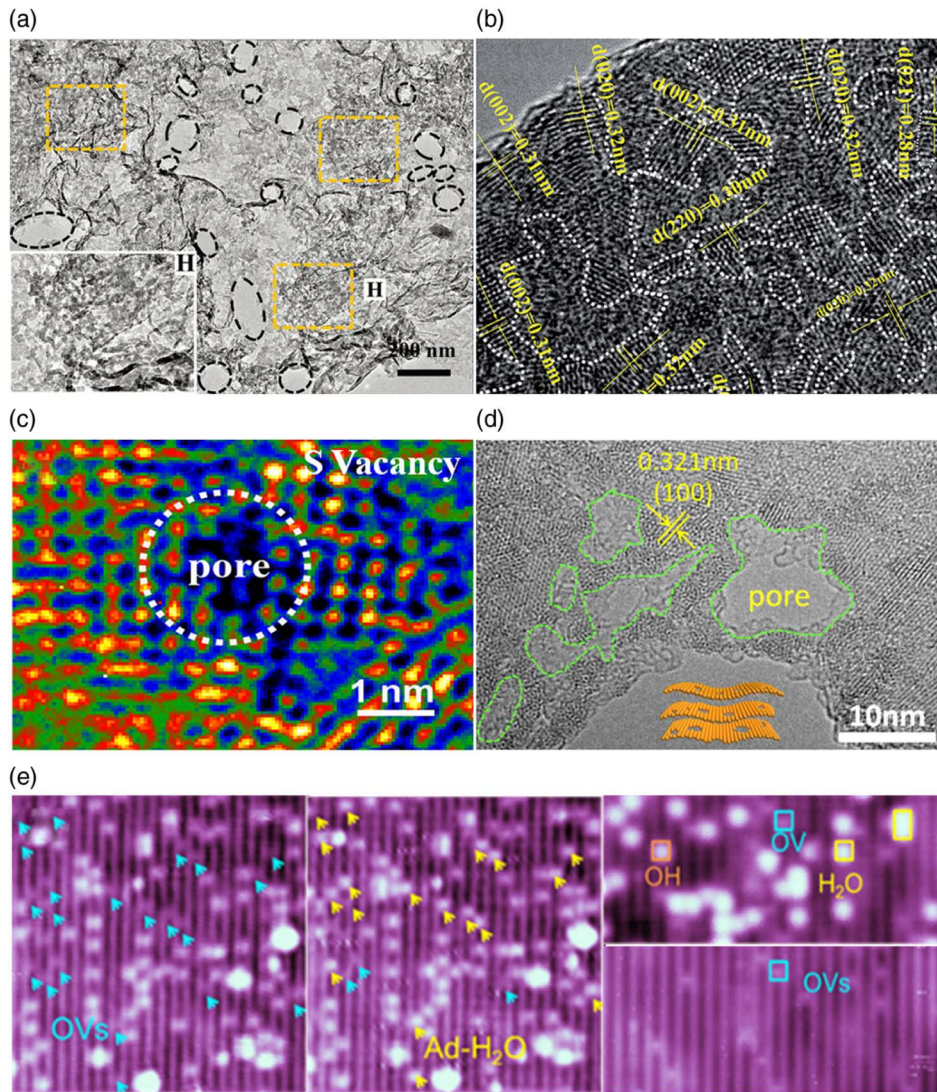


Figure 11. a) TEM image of $\text{g-C}_3\text{N}_4$ nanosheets. Reproduced with permission.^[102] Copyright 2016, Wiley-VCH. b) HRTEM image of $\text{D-ZnS}(\text{en})_{0.5}$. Reproduced with permission.^[105] Copyright 2017, The Royal Society of Chemistry. c) False-color image of HRTEM image of $\text{V}_{\text{s}}\text{-M-ZnIn}_2\text{S}_4$. Reproduced with permission.^[83] Copyright 2018, American Chemical Society. d) HRTEM of $\text{V}_{\text{s}}\text{-ZnIn}_2\text{S}_4$. Reproduced with permission.^[82] Copyright 2019, Elsevier Ltd. e) STM images of hydroxylated TiO_2 surface with OVs and ad- H_2O . Reproduced with permission.^[109] Copyright 2018, American Chemical Society.

could be enhanced by the long-lived electrons, thus improving the performance of PC CO_2 conversion.^[47] Xiong et al. employed ultrafast TA spectroscopy to determine the charge dynamics of Cu_2O and $\text{Cu}_3(\text{BTC})_2/\text{Cu}_2\text{O}$, indicating a preferential way of the electrons, thus boosting PEC CO_2 conversion (Figure 13c).^[114] According to the analysis of TA spectroscopy (Figure 13d), the distribution of charge transfer was confirmed in CdS-Au-TiO_2 .^[115] Up to now, the defective photocatalysts, the synthesized approaches, the types of defects and the techniques have been summarized in Table 2, understanding the difference of various defects and characterization techniques in the photocatalysts. Although substantial achievements have been obtained by use of various characterization techniques for the determination of the defects in the photocatalysis, there

is still enough space to explore new characterization techniques and the detailed information of the defects by the controllable techniques.

6. Application of Defect Engineering for Solar Energy Conversion

Based on the abovementioned analysis, defect engineering plays a pivotal role in solar energy conversion. It is essential to summarize the advanced PC applications, such as solar water splitting, solar CO_2 conversion, nitrogen fixation to ammonia, molecular oxygen activation, pollutants degradation, and solar-driven devices.

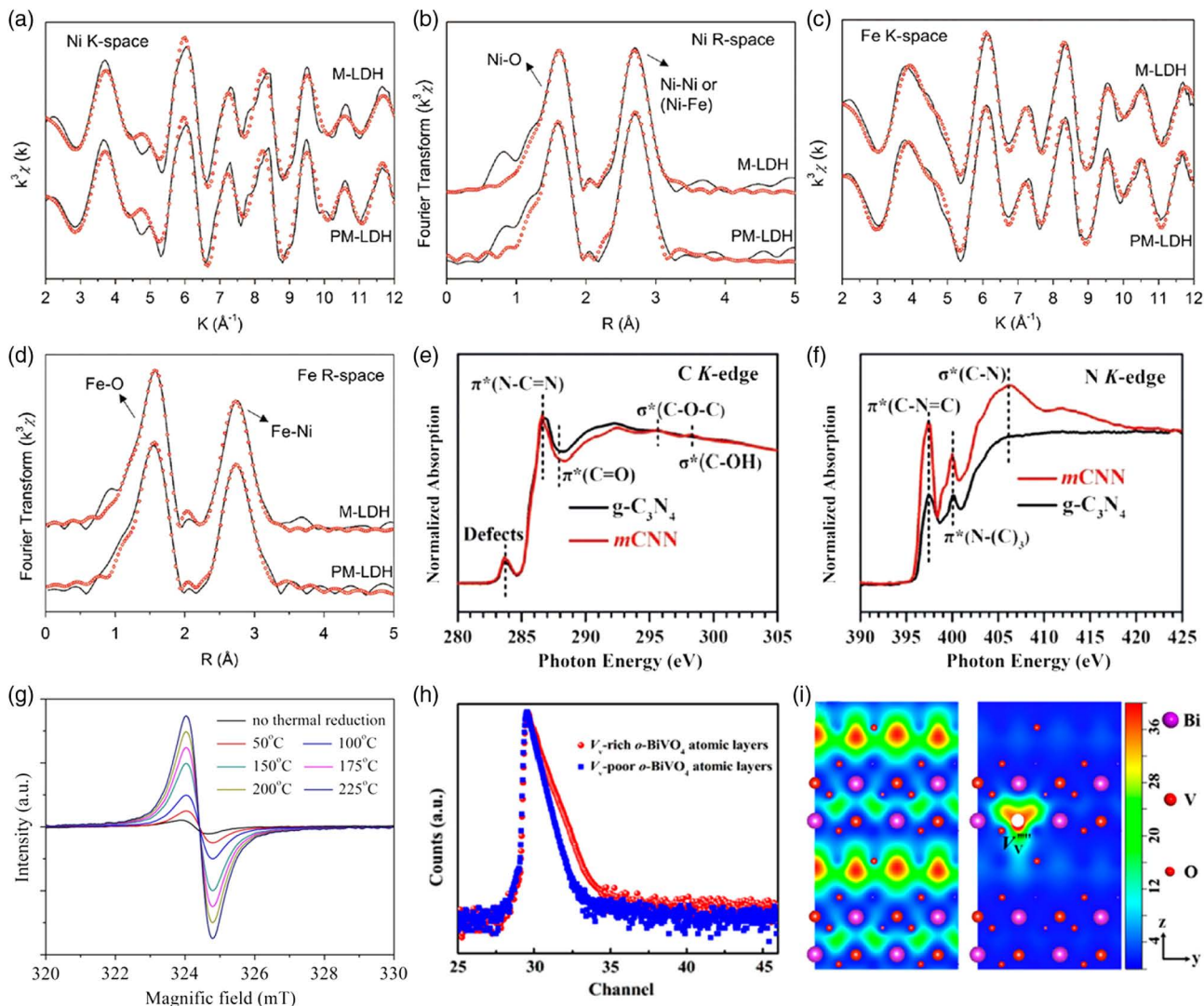


Figure 12. a-d) Ni K-edge and Fe K-edge EXAFS oscillation functions $k^3\chi(k)$ and the corresponding R-space plots for PM-LDH and M-LDH. Reproduced with permission.^[107] Copyright 2019, Wiley-VCH. e,f) XANES spectra of C K-edge and N K-edge for g-C₃N₄ and defective g-C₃N₄. Reproduced with permission.^[108] Copyright 2019, Wiley-VCH. g) EPR spectra of V_x-BWO layers. Reproduced with permission.^[110] Copyright 2019, Elsevier Ltd. h,i) Positron lifetime spectrum and scheme of trapped positrons of defective o-BiVO₄ layers. Reproduced with permission.^[64] Copyright 2018, American Chemical Society.

6.1. PEC Water Splitting

So far, numerous achievements have been obtained by defect engineering, significantly improving the PEC performance of photoelectrodes,^[80,92,116-122] such as Si, TiO₂, WO₃, BiVO₄, Fe₂O₃ and ZnO photoelectrodes. For instance, defect confined in ZrO₂ nanowire photocathode presented a solar-to-hydrogen conversion efficiency of 3.1% and Faradaic efficiency of 97.8% (Figure 14a).^[92] Compared with various photoanodes, as-prepared Nb-doped NiO_x/Ni/black Si photoanode achieved a photocurrent density of 29.1 mA cm⁻² and highest charge separation efficiency of 81% at 1.23 V versus reversible hydrogen (vs RHE) (Figure 14b).^[94] Black core-shell BiVO₄/TiO_{2-x} photoanode through coupling amorphous TiO₂ on BiVO₄ by use of atomic layer deposition and plasma treatment reached 6.6 mA cm⁻² at 1.23 V versus

RHE and a high photon-to-current efficiency of 2.5% due to improved photon absorption and charge separation (Figure 14c).^[116] β-FeOOH/BiVO₄ photoanodes by the integration of 2 nm β-FeOOH nanolayers with abundant OVs showed a remarkable photocurrent density of 4.3 mA cm⁻² at 1.23 V versus RHE (AM 1.5G), promoting the hole transport/trapping and the generation of more active sites for water oxidation (Figure 14d) due to the existence of OVs and ultrathin nanostructures of β-FeOOH.^[117] Compared with In₂S₃, defective In₂O_{3-x}/In₂S₃ photoanode achieved a photocurrent density of 1.28 mA cm⁻² at 1.23 V versus RHE, nearly 21 and 79 times higher than those of In₂S₃ atomic layers and bulk counterpart, respectively.^[80] The OVs and nitrogen were incorporated into bismuth vanadate electrodes by nitrogen treatment and presented the photon-to-current efficiency of 2% due to the efficient regulation of the electronic

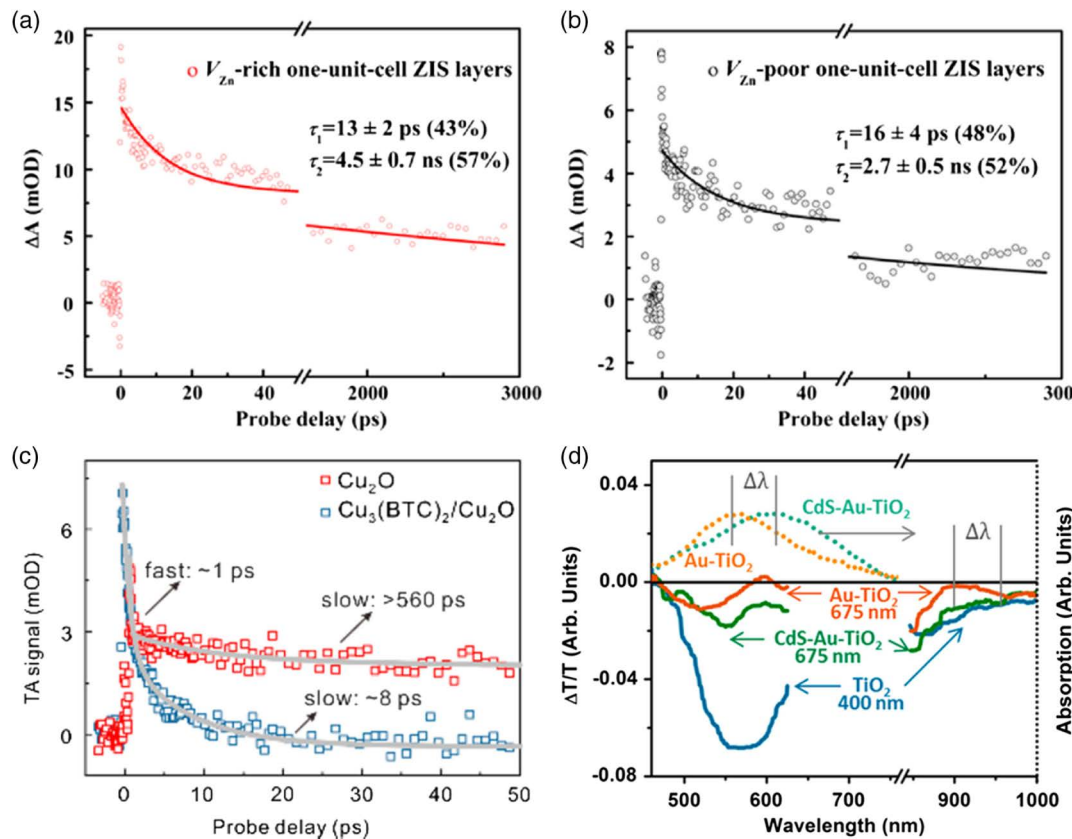


Figure 13. a,b) Ultrafast TA spectroscopy of defective $ZnIn_2S_4$ layers. Reproduced with permission.^[47] Copyright 2017, American Chemical Society. c) Ultrafast TA spectroscopy of Cu_2O and $Cu_3(BTC)_2/Cu_2O$. Reproduced with permission.^[114] Copyright 2019, American Chemical Society. d) Ultrafast TA spectroscopy of CdS -Au-TiO₂. Reproduced with permission.^[115] Copyright 2014, American Chemical Society.

structure and charge transfer by nitrogen doping and OVs.^[118] OVs and tungsten vacancies confined in WO_3 photoanode achieved the improved PEC water oxidation.^[119] Oxygen vacancy confined in $BaSnO_3$ photoanode with the integration of $FeOOH/NiOOH$ cocatalysts presented a remarkable photocurrent density.^[120] As-synthesized hierarchical heterostructures by the integration of SnS_x nanosheets and CdS nanorods presented excellent PEC performance, reaching an extraordinary photocurrent density, due to the protection of CdS and efficient charge separation by the introduction of SnS_x in CdS system.^[121] What is most significant is that the involved hydrogen and oxygen can be separated in the photoanode and the photocathode in this typical PEC cell, indicating the advantage of the PEC system from the issues of purity and safety of the involved products in comparison with the heterogeneous PC system.^[122] Thus, the PEC efficiency could be significantly enhanced due to the efficient regulation of light absorption, charge separation, and PC reactions by defect engineering in the PEC system.

6.2. PC Water Splitting

In a heterogeneous PC system, hydrogen and oxygen can be collected simultaneously, presenting the advantage for practical industrial applications. With regard to the modulation of the

PC water splitting by defect engineering, Wang et al. reported 1D $Cd_{1-x}Zn_xS@O-MoS_2/NiO_x$ hybrids by the integration of oxygen-incorporated MoS_2 ($O-MoS_2$) and NiO_x with abundant defects that endowed a remarkable hydrogen evolution rate of $223.17\text{ mmol h}^{-1}\text{ g}^{-1}$ in Na_2S/Na_2SO_3 solution as the sacrificial agent and an apparent quantum yield of 64.1% at 420 nm as well as outstanding durability (Figure 15a,b).^[123] The heterostructures by the integration of WO_3 and $V_s-ZnIn_2S_4$ with NiS quantum dots reached the high PC hydrogen production rate of $11.09\text{ mmol g}^{-1}\text{ h}^{-1}$ under visible-light irradiation and an apparent quantum efficiency of 72% at 420 nm (Figure 15c,d).^[82] OVs confined in WO_3 achieved a high PC evolution rate, which is ascribed to the promotion of light harvesting due to surface plasmon resonance by the introduction of OVs (Figure 15e).^[70] Surface defects confined in $Zn-Cd-S$ solid solution achieved the outstanding PC hydrogen production rate due to the introduction of sulfur defects by the confirmation of X-ray photoelectron spectra and photoluminescence spectra.^[124] Particularly, Zou et al. reported metal-defected TiO_2 and ZnO semiconductors with abundant metal vacancies,^[44,125,126] presenting a remarkable PC performance and an essential relationship of the defect structure and the PC performance of metal-defected photocatalysts. Although the impressive achievements have been obtained in this PC field, there are still the challenges to the design and the enhancement of active photocatalysts for practical application.

Table 2. Summary of typical defective photocatalysts with different defects and synthesis methods as well as characterization techniques.

Materials	Defect types	Synthesis method	Characterization	Ref.
TiO ₂	OVs/Zr ⁴⁺ dopants	Vacuum annealing	HRTEM, XPS	[31]
TiO ₂	OVs/Ti vacancies	Heat treatment under air	STEM, EPR, XPS	[50]
TiO ₂	Ti ³⁺ dopants	Solvothermal treatment	HRTEM, EPR, XPS	[44]
TiO ₂	Edge dislocation	Hydrothermal reaction	HRTEM, Raman	[51]
TiO ₂	OVs	H ₂ treatment	EPR, XPS	[58]
WO ₃	OVs	Vacuum annealing	HRTEM, XPS, EPR	[32]
Fe ₂ O ₃	OVs	Magnetron sputtering	XPS, Raman	[33]
ZnO	OVs/Zn vacancies	Hydrothermal reaction	XPS, EPR	[49]
BiVO ₄	OVs	Hydrothermal reaction	EPR, XPS, TRFS	[34]
Ga ₂ O ₃	Phase-junctions	Thermal calcination	TA, HRTEM, XPS, Raman	[53]
Bi ₂ O ₃	Phase-junctions	Hydrothermal reaction	HRTEM, XPS	[53]
Bi ₂ WO ₆	OVs/Nb ⁵⁺ dopants	Hydrothermal reaction	HRTEM, XPS, Raman	[59]
Mn _x Co _{3-x} O ₄	Mn-Co vacancies	Thermal calcination	EXAFS, XPS	[48]
Ti _x Ag _{1-x} O ₂	Distortion	Thermal calcination	HRTEM, XPS, EDX	[57]
HNB ₃ O ₈	Lattice disorder	Room temperature reduction	AFM, EPR, XPS, HRTEM	[55]
Bi ₇ O ₉ I ₃	I vacancies	Solvothermal treatment	EPR, XPS	[40]
Bi ₁₂ O ₁₇ Cl ₂	OVs	Solvothermal treatment	HAADF-STEM, EPR, XPS	[35]
BiOBr	OVs	Solvothermal treatment	HRTEM, EPR, XPS	[36]
δ-FeOOH	Fe vacancies	Room temperature reduction	AFM, TEM-STM, EPR, XPS, EXAFS	[46]
SnCoFe hydroxide	Sn vacancies	N ₂ plasma	XANES, EXAFS, STEM	[45]
C ₃ N ₄	C vacancies	NH ₃ treatment	EPR, XPS	[37]
C ₃ N ₄	N vacancies	H ₂ treatment	TRFS, XPS	[38]
TaON	N vacancies	NH ₃ treatment	TA	[39]
ZnS	S vacancies	Room temperature reduction	EPR, XPS	[41]
CdS	S vacancies	Light irradiation	HRTEM, XPS	[42]
CdS	Dislocation	CVD process	HRTEM	[52]
CdSe	Dislocation	CVD process	HRTEM	[52]
ZnIn ₂ S ₄	S vacancies	Chemical reduction	AFM, HRTEM, EPR, TA	[43]
ZnIn ₂ S ₄	Zn vacancies	Hydrothermal reaction	HRTEM, EPR, PAS, HAADF-STEM, XANES	[47]
Cd _{0.5} Zn _{0.5} S	Twin boundaries	Solvothermal treatment	STEM, EDX	[29]

6.3. Solar CO₂ Conversion

Facing global warming and climate change, tremendous attempts have been paid to solar CO₂ conversion to the valuable fuels. Defect engineering is a promising strategy to optimize the reduction performance of solar CO₂ conversion. For example, zinc vacancies confined in ZnIn₂S₄ layers presented superior PC performance for solar CO₂ reduction and outstanding durability due to efficient charge separation by the regulation of the defects (Figure 16a).^[47] Wang et al. developed melon polymeric matrix as a typical polymer semiconductor with carbon vacancies by the confirmation of positron annihilation spectroscopy, achieving the remarkable enhancement of PC CO₂ conversion into CO.^[167] OVs confined in BiOBr layers showed excellent reduction efficiency of visible-light CO₂ conversion due to the enhanced light absorption and charge separation by OVs confirmed by XANES and EPR spectra (Figure 16b).^[127] OVs confined in Bi₂O₃ atomic layers achieved remarkable production

yield of dimethyl carbonate (DMC) by use of CO₂ and CH₃OH under CO₂ pressure due to the improved evolution of •CO²⁻ species by oxygen defects (Figure 16c).^[128] The low efficiency of solar CO₂ conversion is limited due to narrow light absorption and low charge separation for Bi₂WO₆ (BWO). In this work, the phosphate and oxygen vacancy were introduced into BWO layers, narrowing the bandgap from 3.52 to 2.06 eV and enhancing the PC generation rate of methanol of 157 μmol g⁻¹ h⁻¹ (Figure 16d).^[129] Meanwhile, sodium tantalate cubes with oxygen vacancy and nitrogen (V_o-NaTaON) regulated the bandgap from 3.78 to 2.04 eV, and the integration of nitrogen-doped graphene and V_o-NaTaON produced the CH₄ and CO evolution yields of 45 and 180 μmol after 5 h visible-light irradiation (Figure 16e).^[130] Ultrathin CuIn₅S₈ layers with sulfur defects achieved the high visible-light-responsive generation rate of CH₄ from CO₂ conversion and near 100% selectivity of CH₄ due to the generation of a highly stable Cu-C-O-In intermediate at the Cu-In dual sites.^[110] Although various

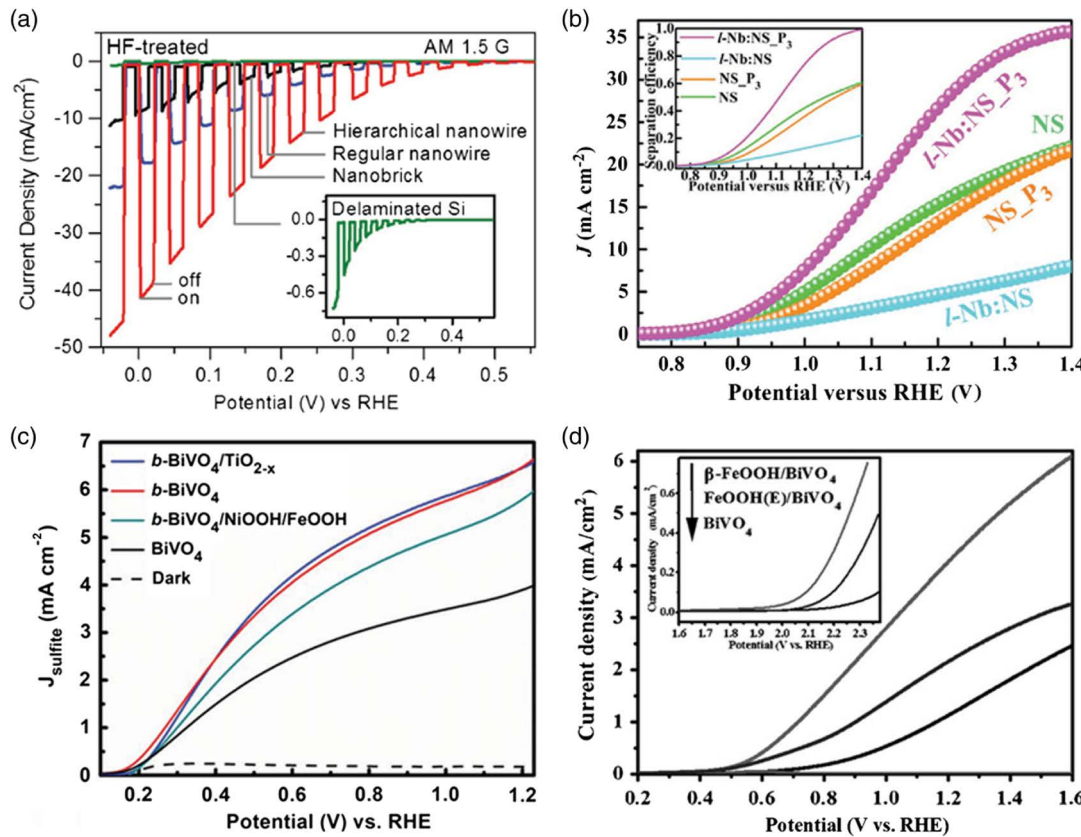


Figure 14. a) LSV curves for HF-treated ZrO_2 film photocathodes. Reproduced with permission.^[92] Copyright 2017, Wiley-VCH. b) LSV curves for Nb-doped $\text{NiO}_x/\text{Ni}/\text{black Si}$. Reproduced with permission.^[94] Copyright 2018, Wiley-VCH. c) LSV curves for $b\text{-BiVO}_4/\text{TiO}_{2-x}$ photoanodes. Reproduced with permission.^[116] Copyright 2019, Wiley-VCH. d) LSV curves for $\beta\text{-FeOOH}/\text{BiVO}_4$ photoanodes. Reproduced with permission.^[117] Copyright 2018, Wiley-VCH.

attempts have been conducted, it is still a long way to design and fabricate the defective photocatalysts with enhanced light absorption and charge separation, enabling efficient solar CO_2 conversion.

6.4. Solar Nitrogen Fixation

Industrially, the fixation of nitrogen to ammonia has been conducted through a conventional Haber–osch process under high temperature and pressure. However, PC nitrogen fixation presents a logical way to develop ammonia synthesis under near-ambient conditions. What deserves to be mentioned the most is that the PC activity of nitrogen fixation could be modulated through defect engineering.^[284–289] For instance, OVs confined in BiOBr nanosheets have been reported, achieving the high NH_3 yield rate of $223.3 \mu\text{mol h}^{-1} \text{g}^{-1}$ for solar N_2 fixation due to the availability of localized electrons for π -back donation by the generation of OVs (Figure 17a).^[131] Meanwhile, OVs confined in $\text{Bi}_5\text{O}_7\text{Br}$ nanotubes presented the NH_3 generation rate of $1.38 \text{ mmol h}^{-1} \text{g}^{-1}$ and an apparent quantum efficiency over 2.3% at 420 nm due to the formation of light-switchable OVs.^[132] OVs confined in TiO_2 nanosheets by the integration of Au nanocrystals generated an excellent N_2 fixation rate of $78.6 \mu\text{mol h}^{-1} \text{g}^{-1}$ and apparent quantum

efficiency of 0.82% at 550 nm.^[133] OVs and intrinsic strain confined in TiO_2 nanosheets produced the outstanding conversion rate, $78.9 \mu\text{mol g}^{-1} \text{h}^{-1}$, for solar N_2 conversion to NH_3 under full solar irradiation. Particularly, solar N_2 reduction rate of $0.72 \mu\text{mol g}^{-1} \text{h}^{-1}$ by use of defective TiO_2 nanosheets was achieved at 600 and 700 nm monochromatic irradiation (Figure 17b).^[66] OVs confined in TiO_2 promoted PC performance of solar N_2 conversion to ammonia with a solar-to-energy conversion efficiency of 0.02%, presenting a mechanism toward N_2 conversion on the surface of Ti^{3+} species (Figure 17c).^[134] CuCr LDH nanosheets with compressive strain and distorted structure produced a robust solar N_2 conversion rate of $184.8 \mu\text{mol g}^{-1} \text{h}^{-1}$ under UV-vis irradiation and $142.9 \mu\text{mol g}^{-1} \text{h}^{-1}$ under visible-light irradiation due to the adsorption and activation of N_2 and H_2O by the introduction of OVs.^[135] Moreover, the surface OVs were tuned by atomic layer deposition, resulting in the formation of the amorphous TiO_2 layer on Au/TiO_2 photoelectrodes and thus promoting the efficiency of PEC N_2 conversion to ammonia (Figure 17d).^[85] Thus, a series of achievements indicated that the unique architecture with abundant defects can effectively tune the local atomic arrangement and electronic structure and thereby enhance the generation rate of solar N_2 conversion to ammonia.

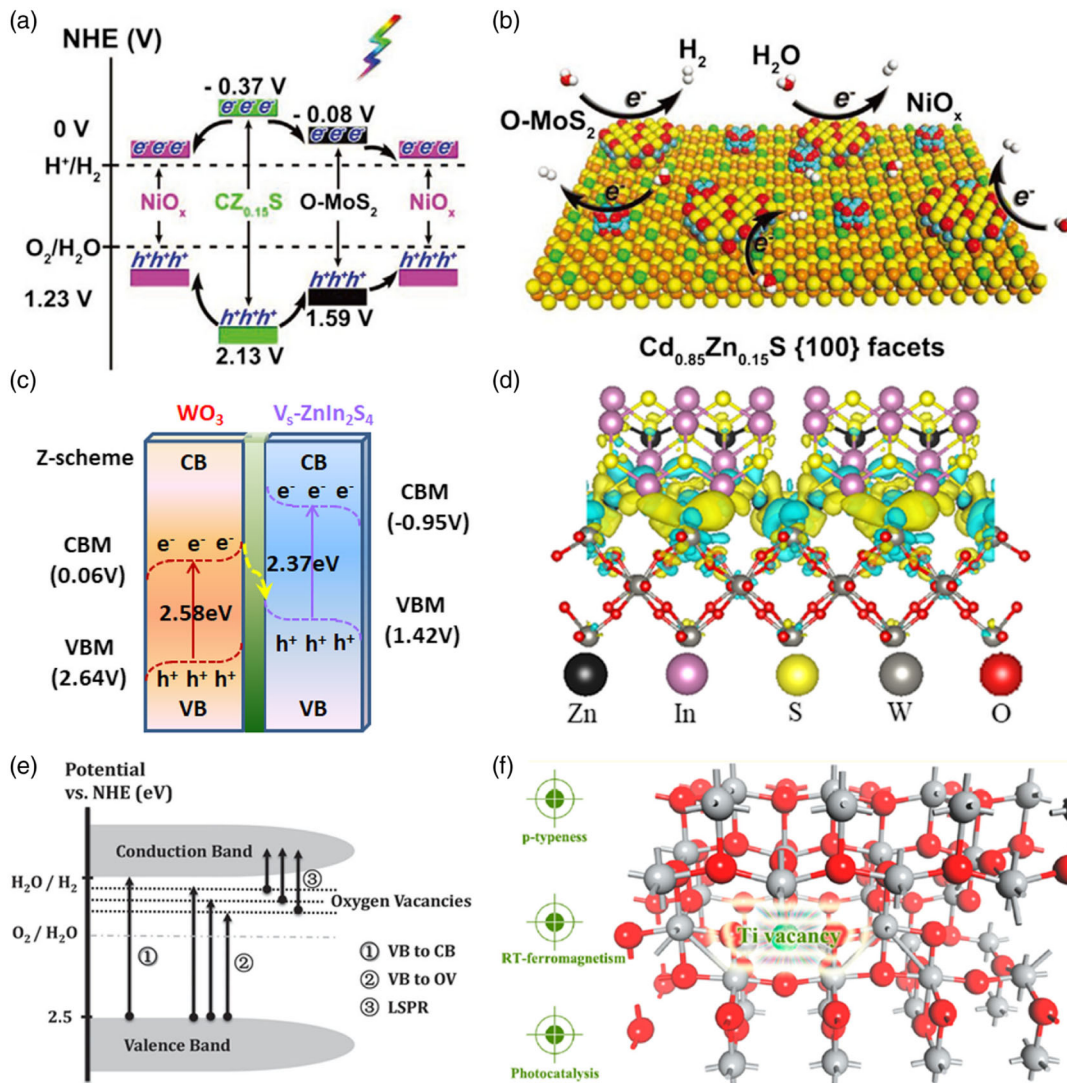


Figure 15. a,b) Energy-band alignments and schematic illustration of solar water splitting over Cd_{1-x}Zn_xS@O-MoS₂/NiO_x hybrids. Reproduced with permission.^[123] Copyright 2019, Wiley-VCH. c,d) Band alignments and 3D charge density difference of V_s-ZnIn₂S₄/WO₃. Reproduced with permission.^[82] Copyright 2019, Elsevier Ltd. e) Bandgap structure of defective WO₃. Reproduced with permission.^[70] Copyright 2015, Wiley-VCH. f) Optimized cell structures of Ti-defected TiO₂. Reproduced with permission.^[275] Copyright 2015, American Chemical Society.

6.5. Molecular Activation

As the application of oxygen molecular as an oxidant is regarded as an environmentally friendly and sustainable approach, the aerobic oxidation reactions are exceedingly important to chemical, agricultural, and pharmaceutical industries. However, as the triplet form of the oxygen ground state under ambient conditions almost cannot straightforwardly take part in the surface catalytic reactions and oxidize reactant molecules, the oxygen molecules activation into activated oxygen species is a challenge for prosperous aerobic oxidative reactions. However, it is a promising solution to realize oxygen molecules activation into highly active species via the use of the photogenerated carriers by the PC process. Inspired by this point, it is necessary to regulate the elaborated superficial active sites and accurate manipulation of the activated oxygen species type by the defective photocatalysts, such as β -In₂S₃, BiO_{2-x},

Bi₂MoO₆, and La_{0.8}Sr_{0.2}CoO₃,^[136] guaranteeing the transfer of photoinduced carriers from semiconductors to oxygen molecules and inhibiting the unnecessary chemical reactions. For example, the 99% selectivity of NO oxidation to nitrate was obtained by blue TiO₂ with abundant OVs under visible irradiation due to the expedited oxygen molecule activation via single-electron pathways to create $\cdot\text{O}_2^-$ species and the accelerated photoinduced carriers consumption induced by the OVs with localized electrons. The created $\cdot\text{O}_2^-$ species could immediately transform the NO molecular to nitrate species, and the carriers consumption restrained the adverse reaction between carriers and NO molecular to avert the toxic NO₂ formation of outgrowth, leading to the highly selective removal of NO molecule.^[137] Moreover, carbon-doped BiO_{2-x} with dual defects (OVs on the surface and oxygen substitutions in the bulk) was fabricated. On the one hand, the lowered conduction band position resulted from surface OVs, acting as active

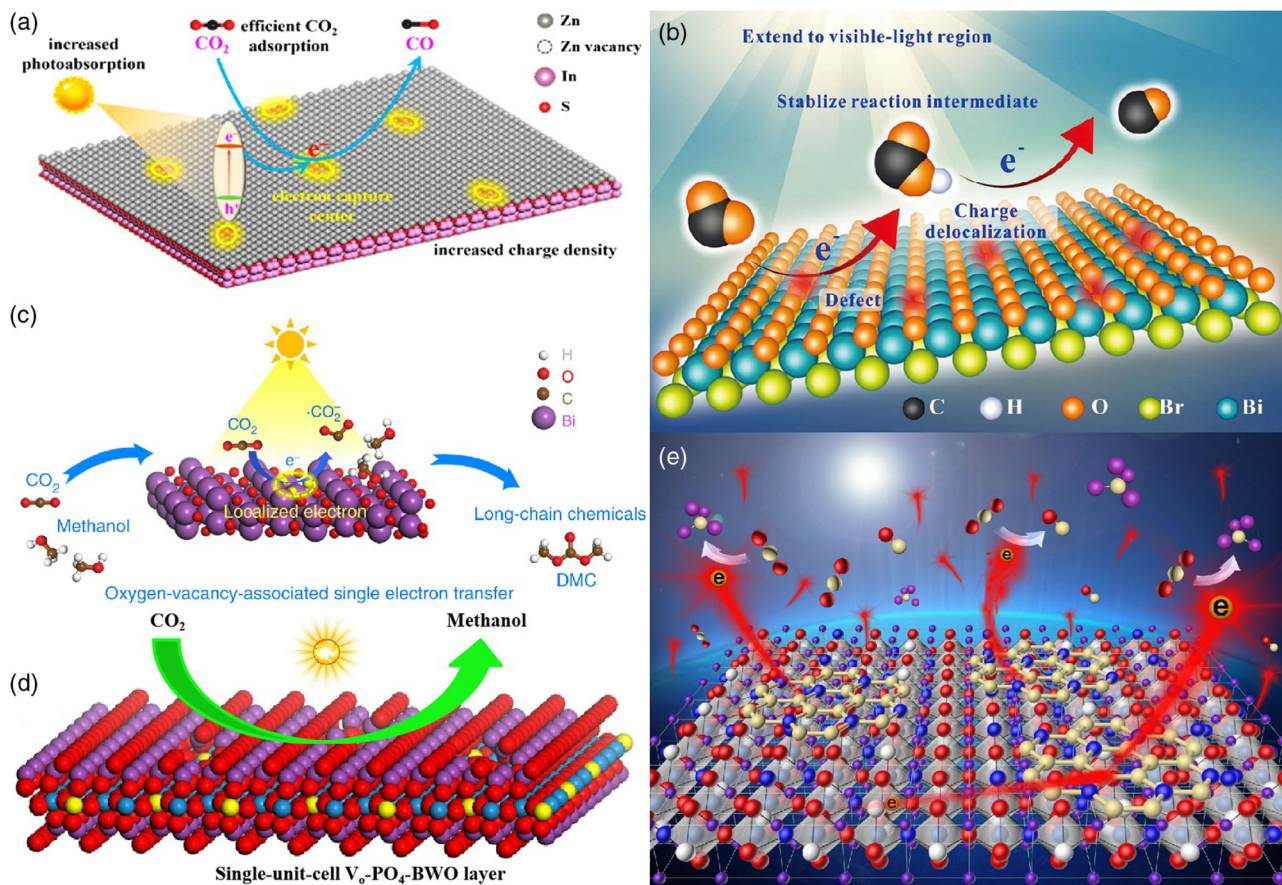


Figure 16. a) Scheme for photoreduction CO₂ on defective ZnIn₂S₄. Reproduced with permission.^[47] Copyright 2017, American Chemical Society. b) Advantages for CO₂ photoreduction over defective BiOBr. Reproduced with permission.^[127] Copyright 2018, Wiley-VCH. c) Scheme for solar CO₂ conversion for defective Bi₂O₃. Reproduced with permission.^[128] Copyright 2019, Nature Publishing Group. d) Scheme of V_x-PO₄-BWO layers for solar CO₂ reduction. Reproduced with permission.^[130] Copyright 2017 Elsevier Ltd. e) Scheme of N-GQDs/V_x-NaTaON for solar CO₂ reduction. Reproduced with permission.^[282] Copyright 2016, Elsevier Ltd.

sites for trapping photoinduced electrons, and consequently expedited the adsorption and activation of molecular oxygen. On the other hand, the strong local electric field due to bulk oxygen substitution could accelerate the photoinduced carrier separation from the bulk to the surface, thus synergistically bringing about the highly efficient PC oxygen molecule activation.^[136] Apart from the above inorganic molecules, it is still useful by defect engineering, enhancing the molecular organic adsorption on catalysts for surface organic catalytic reactions.^[138] In comparison with BiVO₄, oxygen defect-rich BiVO₄ nanotubes exposed with active {010} facets exhibited excellent PC activity for the selective N≡N coupling reaction of 5-amino-1H-tetrazole into sodium 5,5-azotetrazolate due to the enhanced light absorption and efficient charge separation in this architecture.^[138d] Thus, this approach offers an effective strategy for artificial solar energy utilization to chemical energy.

6.6. Pollution Degradation

With the acceleration of industrialization, it is harmful to the ecological environment and human health due to a large number of

environment pollution problems. Photocatalysis has been regarded as a promising strategy for pollutants degradation by use of defect-rich semiconductor materials. For example, porous defective ZnO hexagonal plates were prepared by hydrothermal and high-temperature reduction process, presenting the enhanced solar-driven PC performance of tetracycline degradation due to the visible-light absorption, and promoted electron-hole separation by abundant surface active sites and the surface OV defects.^[139] The distorted graphitic carbon nitride with markedly reinforced π-π* and n-π* electron transitions was synthesized by a novel isopropanol-assisted solvothermal-copolymerization strategy, exhibiting the outstanding PC degradation performance of rhodamine B under visible-light irradiation due to visible-light (photon) adsorption and photoinduced carrier transfer by the meliorative structure and energy level configuration.^[139] The doubly surface-modified BiOIO₃ was produced by the microwave reaction process using ethylene glycol, acting as a reducing agent to in situ generate iodine ions and OVs. The excellent visible-light PC performance for the degradation of several model pollutants, such as parabens, rhodamine B, bisphenol A, and 4-hydroxybenzoic acid has been

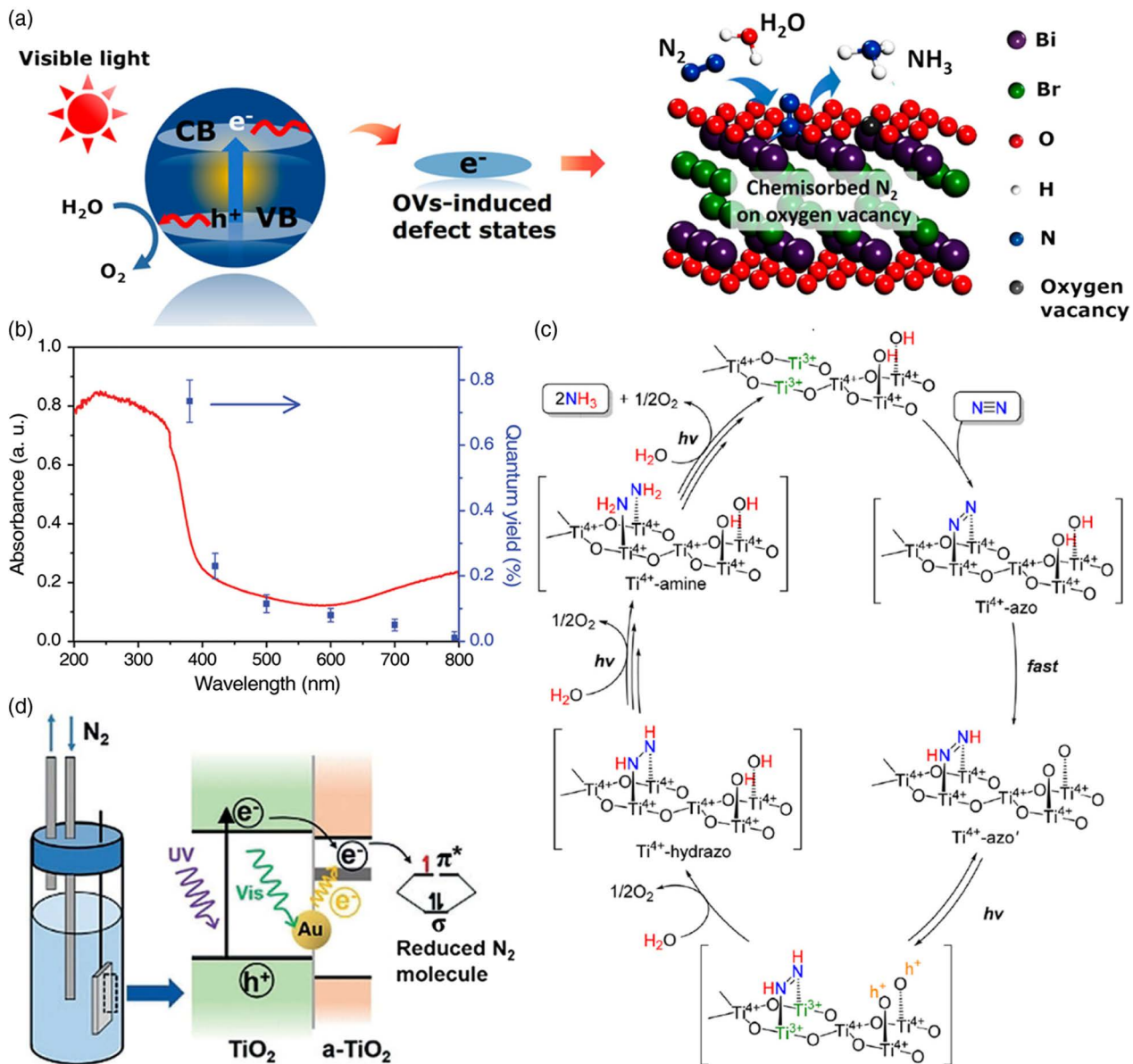


Figure 17. a) Schematic illustration of solar N_2 fixation of BiOBr . Reproduced with permission.^[131] Copyright 2015, American Chemical Society. b) UV–vis diffuse reflectance spectra and quantum efficiency of defective TiO_2 for N_2 reduction. Reproduced with permission.^[66] Copyright 2019, Wiley-VCH. c) Mechanism for solar N_2 fixation of defective TiO_2 . Reproduced with permission.^[133] Copyright 2017, American Chemical Society. d) Illustration of N_2 reduction on defective TiO_2 electrode. Reproduced with permission.^[85] Copyright 2018, Wiley-VCH.

explored due to the appropriate band gaps by the introducing defect energy levels and the key reactive species of the photogenerated h^+ and $\cdot\text{O}_2^-$ radicals.^[139] Therefore, photocatalysis is proven as an efficient and environmentally friendly treatment technique of pollution degradation by defect engineering.

6.7. Solar-Driven Devices

As is well known, it is interesting to explore next-generation solar cells with low cost and high efficiency. Typically, the light absorption and charge transport play an important role upon the optimization of solar energy conversion. Among various metal halide

perovskite solar cells, it is essential to regulate the charge transport from the perovskite absorber to the respective electrodes through electron and hole transport layers. TiO_2 is the most commonly used charge transport material, it is a challenge to explore desirable TiO_2 . For instance, amorphous, OVs containing the TiO_2 buffer layer was intimately situated on the surface of anatase TiO_2 , constructing the bridge at the interface between TiO_2 electron transport layer (ETL) and the perovskite absorber. It is worth mentioning that the introduction of abundant OVs could effectively promote electron transfer from perovskite to acid-treated TiO_2 ETL and prevent the recombination of the photoexcited electron–hole, presenting an improved short-circuit current

and power conversion efficiency.^[140] Moreover, OV confined in TiO₂ and ZnO nanorods arrays on fluorine-doped SnO₂-coated glass were synthesized by hydrothermal and hydrogenation routes. High efficiencies of both dye and Sb₂S₃-sensitized solar cells by use of defective TiO₂ and ZnO nanorods arrays were achieved due to the enhanced photoconductivity by defect engineering.^[140] Furthermore, MoO₃ film with OVs induced by the hydroxyl group by a simple low-temperature-processed solution approach facilitates the hole transport from the photoactive layer to the anode in organic solar cells due to effective hole transporting and electron blocking features, desirable electrical conductivity, and environmental stability. Especially, the power conversion efficiency over 10% was obtained in molybdenum oxide-based organic solar cells.^[140] Therefore, the achievements provide in-depth insights toward designing and promoting solar conversion performance through defect engineering.

7. Conclusions

Defect engineering presents great potential for numerous solar energy conversion applications, thus drawing unprecedented attention in recent years. Indeed, defect engineering provides a promising approach to tailor light absorption of semiconductors, optimize charge separation, and maneuver surface reactions, thus leading to the enhanced PC activities for versatile applications. The recent progress of defect engineering is summarized for solar energy conversion. Taking the defect classification as the beginning, the definition of various defects, the synthesized strategies, and characterization techniques of the controllable defects are presented. The role of defect engineering on solar energy conversion is developed, extending light absorption, promoting charge separation, and facilitating a stable PC reaction. Typically, the achievement of photocatalysts with the defects has been discussed toward versatile applications such as solar water splitting, CO₂ reduction, nitrogen fixation, molecular activation, pollutants degradation, and even solar cells.

Although substantial achievements have been conducted for solar energy conversion by defect engineering, there is still a challenge upon the design, synthesis, and solar energy application. The rational structures of the defects still can be designed according to the types of defects and disadvantages of defects as well as the demands of the PC reactions. To precisely control the defects in photocatalysis, the tunable approaches should be chosen by considering the structures of the defective photocatalysts and types of the defects. To understand the atomic structures of the defects and obtain the valuable insights of the defective photocatalysts, the controllable characterization techniques can be applied to determine the in-depth information on the defects.

However, there are still several challenges to determine the in-depth information of tunable defects in photocatalysis. First, the synthesis, the characterization, and the PC performance of photocatalysts by defect engineering as the challenge have been finished by various groups, so it is hard to understand the comparability of different data depending on the different set-up in photocatalysis. Second, it is essential to design and synthesize the defective photocatalysts according to the types of the defects, establishing a bridge between the types of defects and the activities of catalysts. Third, it is indispensable to develop pivot

characterization techniques, acquiring the precise information of the structures of defects and constructing the relationship between the structure and the performance of the defective photocatalysts. Especially, it still lacks the methods for the visualization and quantification of the defects in the photocatalysts. Fourth, the in-depth mechanism of the defective photocatalysts still remains a challenge, determining the precise roles of light absorption, charge separation, charge lifetimes, and catalytic reactions and building an intimate relationship among the types of defects and the catalysts and the key factors in the photocatalysis. Fifth, it is a big challenge to control the stability of the defects and the defective photocatalysts toward practical applications. Based on the recent progress and future outlook of defect engineering, it is a hot topic for solar energy conversion by defect engineering; thus, we believe that the essential development of the defective photocatalysts could promote the contribution to the progress of practical utilization of solar energy.

Acknowledgements

This work was supported by National Science Foundation of China (no. 21972015, 51672034), the Fundamental Research Funds for the Central Universities (no. DUT20TD06), the Swedish Energy Agency, and the K&A Wallenberg Foundation.

Conflict of Interest

The authors declare no conflict of interest.

Keywords

charge separation, defect engineering, light absorption, photocatalytic reactions, solar energy conversions

Received: October 30, 2019

Revised: December 15, 2019

Published online: January 29, 2020

- [1] X. Li, J. G. Yu, M. Jaroniec, X. B. Chen, *Chem. Rev.* **2019**, *119*, 3962.
- [2] Y. Wang, H. Suzuki, J. Xie, O. Tomita, D. J. Martin, M. Higashi, D. Kong, R. Abe, J. W. Tang, *Chem. Rev.* **2018**, *118*, 5201.
- [3] Y. Ma, X. L. Wang, Y. S. Jia, X. B. Chen, H. X. Han, C. Li, *Chem. Rev.* **2014**, *114*, 9987.
- [4] Y. F. Zhao, G. I. N. Waterhouse, G. B. Chen, X. Y. Xiong, L. Z. Wu, C. H. Tung, T. R. Zhang, *Chem. Soc. Rev.* **2019**, *48*, 1972.
- [5] a) N. Zhang, C. Gao, Y. Xiong, *J. Energy Chem.* **2019**, *37*, 43; b) R. Shi, Y. Zhao, G. Waterhouse, S. Zhang, T. Zhang, *ACS Catal.* **2019**, *9*, 9739; c) S. Zhang, Y. Zhao, R. Shi, G. Waterhouse, T. Zhang, *EnergyChem* **2019**, *1*, 100013; d) H. Wang, X. Sun, D. Li, X. Zhang, S. Chen, W. Shao, Y. Tian, Y. Xie, *J. Am. Chem. Soc.* **2017**, *139*, 2468; e) H. Wang, D. Yong, S. Chen, S. Jiang, X. Zhang, W. Shao, Q. Zhang, W. Yan, B. Pan, Y. Xie, *J. Am. Chem. Soc.* **2018**, *140*, 1760; f) M. Wang, G. Tan, D. Zhang, B. Li, L. Lv, Y. Wang, H. Ren, X. Zhang, A. Xia, Y. Liu, *Appl. Catal., B* **2019**, *254*, 98.
- [6] a) S. Bai, N. Zhang, C. Gao, Y. Xiong, *Nano Energy* **2018**, *53*, 296; b) Y. Liu, C. Xiao, Z. Li, Y. Xie, *Adv. Energy Mater.* **2016**, *6*, 1600436; c) Z. Zheng, Z. Fang, X. Ye, X. Yao, X. Fu, S. Lin, P. Liu, *Nanoscale* **2015**, *7*, 17488; d) H. Li, L. Zhang, *Nanoscale* **2014**, *6*, 7805.

- [7] a) D. J. Martin, G. G. Liu, S. J. A. Moniz, Y. P. Bi, A. M. Beale, J. H. Ye, J. W. Tang, *Chem. Soc. Rev.* **2015**, *44*, 7808; b) H. Li, H. Zhou, K. Chen, K. Liu, S. Li, K. Jiang, W. Zhang, Y. Xie, Z. Cao, H. Li, H. Liu, X. Xu, H. Pan, J. Hu, D. Tang, X. Qiu, J. Fu, M. Liu, *Sol. RRL* **2020**, 1900416, <https://doi.org/10.1002/solr.201900416>; c) J. Pan, Z. Dong, Z. Jiang, C. Zhao, B. Wang, W. Zhao, J. Wang, C. Song, Y. Zheng, C. Li, *Sol. RRL* **2020**, 1900337, <https://doi.org/10.1002/solr.201900337>.
- [8] a) M. Dan, A. Prakash, Q. Cai, J. Xiang, Y. Ye, Y. Li, S. Yu, Y. Lin, Y. Zhou, *Sol. RRL* **2019**, *3*, 1800237; b) Q. Xu, B. Zhu, C. Jiang, B. Cheng, J. Yu, *Sol. RRL* **2018**, *2*, 1800006; c) B. Zhu, L. Zhang, B. Cheng, J. Yu, *Appl. Catal., B* **2018**, *2241*, 98332; d) B. Zhu, B. Cheng, L. Zhang, J. Yu, *Carbon Energy* **2019**, *1*, 32.
- [9] a) R. Shi, G. Waterhouse, T. R. Zhang, *Sol. RRL* **2017**, *1*, 1700126; b) Y. Xiong, Y. Chen, N. Yang, C. Jin, Q. Sun, *Sol. RRL* **2019**, *3*, 1800341.
- [10] Y. J. Yuan, Z. T. Yu, D. Q. Chen, Z. G. Zou, *Chem. Soc. Rev.* **2017**, *46*, 603.
- [11] F. Yang, M. Liu, X. Chen, Z. Xu, H. Zhao, *Sol. RRL* **2018**, *2*, 1800215.
- [12] L. Q. Jing, W. Zhou, G. H. Tian, H. G. Fu, *Chem. Soc. Rev.* **2013**, *42*, 9509.
- [13] a) X. Wang, L. Wu, Z. Wang, H. Wu, X. Zhou, H. Ma, H. Zhong, Z. Xing, G. Cai, C. Jiang, F. Ren, *Sol. RRL* **2019**, *3*, 1800298; b) N. Zhang, M. Q. Yang, S. Q. Liu, Y. G. Sun, Y. J. Xu, *Chem. Rev.* **2015**, *115*, 10307.
- [14] J. Zhu, G. Cheng, J. Xiong, W. Li, S. Dou, *Sol. RRL* **2019**, *3*, 1900256.
- [15] S. Ning, X. Shi, H. Zhang, H. Lin, Z. Zhang, J. Long, Y. Li, X. Wang, *Sol. RRL* **2019**, *3*, 1900059.
- [16] J. Pan, Z. Dong, Z. Jiang, C. Zhao, B. Wang, W. Zhao, J. Wang, C. Song, Y. Zheng, C. Li, *Sol. RRL* **2019**, 1900337.
- [17] J. Hou, Y. Wu, B. Zhang, S. Cao, Z. Li, L. Sun, *Adv. Funct. Mater.* **2019**, *29*, 1808367.
- [18] a) Y. Wu, Y. Meng, J. Hou, S. Cao, Z. Wu, L. Sun, *Adv. Funct. Mater.* **2018**, *28*, 1801397; b) J. Hou, B. Zhang, Z. Li, S. Cao, Y. Sun, Y. Wu, Z. Gao, L. Sun, *ACS Catal.* **2018**, *8*, 4612; c) J. Hou, Y. Wu, S. Cao, Y. Sun, L. Sun, *Small* **2017**, *13*, 1702018.
- [19] J. Hou, Y. Sun, Z. Li, B. Zhang, S. Cao, Y. Wu, Z. Gao, L. Sun, *Adv. Funct. Mater.* **2018**, *28*, 1803278.
- [20] H. Chen, C. Chen, R. Liu, L. Zhang, J. Zhang, D. Wilkinsone, *Chem. Soc. Rev.* **2012**, *41*, 5654.
- [21] J. Hou, H. Cheng, O. Takeda, H. Zhu, *Energy Environ. Sci.* **2015**, *8*, 1348.
- [22] J. Hou, C. Yang, H. Cheng, S. Jiao, O. Takeda, H. Zhu, *Energy Environ. Sci.* **2014**, *7*, 3758.
- [23] J. Hou, H. Cheng, O. Takeda, H. Zhu, *Angew. Chem., Int. Ed.* **2015**, *54*, 8480.
- [24] H. L. Wang, L. S. Zhang, Z. G. Chen, J. Q. Hu, S. J. Li, Z. H. Wang, J. S. Liu, X. C. Wang, *Chem. Soc. Rev.* **2014**, *43*, 5234.
- [25] J. Hu, X. Zhao, W. Chen, Z. Chen, *ACS Omega* **2018**, *3*, 14973.
- [26] W. Zhang, L. Song, J. Cen, M. Liu, *J. Phys. Chem. C* **2019**, *123*, 20730.
- [27] I. Shintaro, K. Namhoon, E. Elif, T. Sakae, I. Tatsumi, *J. Am. Chem. Soc.* **2015**, *137*, 239.
- [28] P. Ren, M. Song, J. Lee, J. Zheng, D. Li, *Adv. Mater. Interfaces* **2019**, 1901121.
- [29] M. Liu, D. Jing, Z. Zhou, L. Guo, *Nat. Commun.* **2013**, *4*, 2278.
- [30] F. Liu, R. Shi, Z. Wang, Y. Weng, Y. Chen, *Angew. Chem., Int. Ed.* **2019**, *58*, 11791.
- [31] M. Shaddad, D. Cardenas-Morcoso, M. García-Tecedor, F. Fabregat-Santiago, J. Bisquert, A. Al-Mayouf, S. Gimenez, *ACS Omega* **2019**, *4*, 16095.
- [32] S. Huang, Y. Long, S. Ruan, Y. Zeng, *ACS Omega* **2019**, *4*, 15593.
- [33] L. Christian, K. Andreas, J. Wolfram, *Nat. Commun.* **2019**, *9*, 4309.
- [34] T. Wei, Y. Zhu, Z. Gu, X. An, L. Liu, Y. Wu, H. Liu, J. Tang, J. Qu, *Nano Energy* **2018**, *51*, 764.
- [35] J. Di, C. Zhu, M. Ji, M. Duan, R. Long, C. Yan, K. Gu, J. Xiong, Y. She, J. Xia, H. Li, Z. Liu, *Angew. Chem., Int. Ed.* **2019**, *57*, 14847.
- [36] H. Li, J. Shang, Z. Ai, L. Zhang, *J. Am. Chem. Soc.* **2015**, *137*, 6393.
- [37] M. Shen, L. Zhang, M. Wang, J. Tian, X. Jin, L. Guo, L. Wang, J. Shi, *J. Mater. Chem. A* **2019**, *7*, 1556.
- [38] P. Niu, L. C. Yin, Y. Q. Yang, G. Liu, H. M. Cheng, *Adv. Mater.* **2014**, *26*, 8046.
- [39] J. Feng, H. Huang, T. Fang, X. Wang, S. Yan, W. Luo, T. Yu, Y. Zhao, Z. Li, Z. Zou, *Adv. Funct. Mater.* **2019**, *29*, 1808389.
- [40] Y. Wei, H. Su, Y. Zhang, L. Zheng, Y. Pan, C. Su, W. Geng, M. Long, *Chem. Eng. J.* **2019**, *375*, 121971.
- [41] H. Pang, X. Meng, P. Li, K. Chang, W. Zhou, X. Wang, X. Zhang, W. Jevasuwan, N. Fukata, D. Wang, J. Ye, *ACS Energy Lett.* **2019**, *4*, 1387.
- [42] X. Yin, L. Li, M. Liu, D. Li, L. Shang, J. Dou, *Chem. Eng. J.* **2019**, *370*, 305.
- [43] Z. W. Li, J. G. Hou, B. Zhang, S. Y. Cao, Y. Z. Wu, Z. M. Gao, X. W. Nie, L. C. Sun, *Nano Energy* **2019**, *59*, 537.
- [44] S. B. Wang, L. Pan, J. J. Song, W. B. Mi, J. J. Zou, L. Wang, X. W. Zhang, *J. Am. Chem. Soc.* **2015**, *137*, 2975.
- [45] D. Chen, M. Qiao, Y. R. Lu, L. Hao, D. Liu, C. L. Dong, Y. Li, S. Wang, *Angew. Chem., Int. Ed.* **2018**, *57*, 8691.
- [46] B. Liu, Y. Wang, H. Peng, R. Yang, Z. Jiang, X. Zhou, C. Lee, H. Zhao, W. Zhang, *Adv. Mater.* **2018**, *30*, 1803144.
- [47] X. Jiao, Z. Chen, X. Li, Y. Sun, S. Gao, W. Yan, C. Wang, Q. Zhang, Y. Lin, Y. Luo, *J. Am. Chem. Soc.* **2017**, *139*, 7586.
- [48] K. Li, R. Zhang, R. Gao, G. Q. Shen, L. Pan, Y. Yao, K. Yu, X. Zhang, J. J. Zou, *Appl. Catal., B* **2019**, *244*, 536.
- [49] S. Wang, C. Y. Huang, L. Pan, Y. Chen, X. Zhang, J. J. Zou, *Catal. Today* **2019**, *335*, 151.
- [50] S. M. Wu, X. L. Liu, X. L. Lian, G. Tian, C. Janiak, Y. X. Zhang, Y. Lu, H. Z. Yu, J. Hu, H. Wei, *Adv. Mater.* **2018**, *30*, 1802173.
- [51] S. I. Cha, H. Kyu Hyeon, K. Y. Hyun, Y. M. Ju, S. Seon Hee, S. Y. Ji, M. Jeong Hyun, L. D. Yoon, *Nanoscale* **2013**, *5*, 753.
- [52] H. Wu, F. Meng, L. Li, S. Jin, G. Zheng, *ACS Nano* **2012**, *6*, 4461.
- [53] a) J. Hou, C. Yang, Z. Wang, W. Zhou, S. Jiao, H. Zhu, *Appl. Catal., B* **2013**, *142–143*, 504; b) X. Wang, Q. Xu, M. Li, S. Shen, X. Wang, Y. Wang, Z. Feng, J. Shi, H. Han, C. Li, *Angew. Chem., Int. Ed.* **2012**, *51*, 13089.
- [54] a) Y. Sun, Q. Liu, S. Gao, H. Cheng, F. Lei, Z. Sun, Y. Jiang, H. Su, S. Wei, Y. Xie, *Nat. Commun.* **2013**, *4*, 2899; b) Y. Liu, X. Hua, C. Xiao, T. Zhou, P. Huang, Z. Guo, B. Pan, Y. Xie, *J. Am. Chem. Soc.* **2016**, *138*, 5087.
- [55] M. Q. Yang, L. Shen, Y. Lu, S. W. Chee, X. Lu, X. Chi, Z. Chen, Q. H. Xu, U. Mirsaidov, G. W. Ho, *Angew. Chem., Int. Ed.* **2019**, *58*, 3077.
- [56] K. Yang, X. Chen, Z. Zheng, J. Wan, M. Feng, Y. Yu, *J. Mater. Chem. A* **2019**, *7*, 3863.
- [57] M. Mathpal, A. Tripathi, P. Kumar, V. Agrahari, M. Singh, A. Agarwal, *Chem. Phys. Lett.* **2014**, *614*, 162.
- [58] J. Lim, Y. Yang, M. R. Hoffmann, *Environ. Sci. Technol.* **2019**, *53*, 6972.
- [59] H. Chen, C. Zhang, Y. Pang, Q. Shen, Y. Yu, Y. Su, J. Wang, F. Zhang, H. Yang, *RSC Adv.* **2019**, *9*, 22559.
- [60] Y. Liu, Y. Li, S. Yang, Y. Lin, J. Zuo, H. Liang, F. Peng, *Chemsuschem* **2018**, *11*, 2766.
- [61] C. Shihai, F. Bin, F. Yanchao, C. Huan, J. Fang, W. Xin, *Chem. Eng. J.* **2018**, *353*, 147.
- [62] H. Wang, Y. Bu, G. Wu, X. Zou, *Dalton Trans.* **2019**, *68*, 11724.
- [63] X. Li, Y. Cheng, Q. Wu, J. Xu, Y. Wang, *Appl. Catal., B* **2019**, *240*, 270.
- [64] S. Gao, B. Gu, X. Jiao, Y. Sun, X. Zu, F. Yang, W. Zhu, C. Wang, Z. Feng, B. Ye, Y. Xie, *J. Am. Chem. Soc.* **2017**, *139*, 3438.
- [65] J. Wu, N. Li, H. B. Fang, X. Li, Y. Z. Zheng, X. Tao, *Chem. Eng. J.* **2019**, *35*, 20.

- [66] Y. Zhao, Y. Zhao, R. Shi, B. Wang, G. I. N. Waterhouse, L.-Z. Wu, C.-H. Tung, T. Zhang, *Adv. Mater.* **2019**, *31*, 1806482.
- [67] S. U. Khan, M. Alshahry, I. W. Ingler Jr, *Science* **2002**, *297*, 2243.
- [68] I. S. Cho, M. Logar, H. L. Chi, L. Cai, F. B. Prinz, X. Zheng, *Nano Lett.* **2014**, *14*, 24.
- [69] D. Zhou, X. Xiong, Z. Cai, N. Han, Y. Jia, Q. Xie, X. Duan, T. Xie, X. Zheng, X. Sun, X. Duan, *Small Methods* **2018**, *2*, 1800083.
- [70] J. Yan, T. Wang, G. Wu, W. Dai, N. Guan, L. Li, J. Gong, *Adv. Mater.* **2015**, *27*, 1580.
- [71] P. Yang, H. Zhuzhang, R. Wang, W. Lin, X. Wang, *Angew. Chem., Int. Ed.* **2019**, *58*, 1134.
- [72] J. Y. Zheng, Y. H. Lyu, R. L. Wang, C. Xie, H. J. Zhou, S. P. Jiang, S. Y. Wang, *Nat. Commun.* **2018**, *9*, 3572.
- [73] J. Yabin, S. Zongzhao, T. Chao, Z. Yuxia, Z. Lei, H. Limin, *Appl. Catal., B* **2019**, *240*, 30.
- [74] F. Lei, Y. Sun, K. Liu, G. Shan, L. Liang, B. Pan, X. Yi, *J. Am. Chem. Soc.* **2014**, *136*, 6826.
- [75] Y. Liu, L. Lin, X. Chong, X. Hua, L. Zhou, B. Pan, X. Yi, *Adv. Energy Mater.* **2016**, *6*, 1600437.
- [76] S. Gao, Y. Sun, F. Lei, L. Liang, J. Liu, W. Bi, B. Pan, Y. Xie, *Angew. Chem., Int. Ed.* **2015**, *46*, 12789.
- [77] J.-W. Zhang, S. Gong, N. Mahmood, L. Pan, X. Zhang, J.-J. Zou, *Appl. Catal., B* **2018**, *221*, 9.
- [78] Q. Yuan, D. Liu, N. Zhang, W. Ye, H. Ju, L. Shi, R. Long, J. Zhu, Y. Xiong, *Angew. Chem., Int. Ed.* **2017**, *129*, 4206.
- [79] J. Di, X. Zhao, C. Lian, M. Ji, J. Xia, J. Xiong, W. Zhou, X. Cao, Y. She, H. Liu, *Nano Energy* **2019**, *61*, 54.
- [80] a) J. G. Hou, S. Y. Cao, Y. Q. Sun, Y. Z. Wu, F. Liang, Z. S. Lin, L. C. Sun, *Adv. Energy Mater.* **2018**, *8*, 1701114; b) S. Cao, Y. Wu, J. Hou, B. Zhang, Z. Li, X. Nie, L. Sun, *Adv. Energy Mater.* **2020**, 1902935, <https://doi.org/10.1002/aenm.201902935>.
- [81] Y. Bi, Y. Zhang, Z. Xu, G. Li, W. Hao, *Angew. Chem., Int. Ed.* **2018**, *6*, 23283.
- [82] Z. W. Li, J. G. Hou, B. Zhang, S. Y. Cao, Y. Z. Wu, Z. M. Gao, X. W. Nie, L. C. Sun, *Nano Energy* **2019**, *59*, 537.
- [83] S. Zhang, X. Liu, C. Liu, S. Luo, L. Wang, T. Cai, Y. Zeng, J. Yuan, W. Dong, Y. Pei, *ACS Nano* **2017**, *12*, 751.
- [84] Y. Zhu, L. Wang, Y. Liu, L. Shao, X. Xia, *Appl. Catal., B* **2019**, *241*, 483.
- [85] C. Li, T. Wang, Z. J. Zhao, W. Yang, J. Li, A. Li, Z. Yang, G. A. Ozin, J. Gong, *Angew. Chem., Int. Ed.* **2018**, *57*, 5278.
- [86] Y. Zhu, L. Qiang, Y. Liu, W. Hua, Y. Zhu, *Appl. Catal., B* **2016**, *187*, 204.
- [87] G. Liu, L. C. Yin, J. Q. Wang, P. Niu, C. Zhen, Y. P. Xie, H. M. Cheng, *Energy Environ. Sci.* **2012**, *5*, 9603.
- [88] Y. Q. Yang, L. C. Yin, Y. Gong, P. Niu, J. Q. Wang, L. Gu, X. Q. Chen, G. Liu, L. Z. Wang, H. M. Cheng, *Adv. Mater.* **2018**, *30*, 1704479.
- [89] X. Hong, J. Tan, H. Zhu, N. Feng, Y. Yang, J. Irvine, L. Wang, G. Liu, H. M. Cheng, *Chem. Eur. J.* **2019**, *25*, 1787.
- [90] H. J. Yu, R. Shi, Y. X. Zhao, T. Bian, Y. F. Zhao, C. Zhou, G. I. N. Waterhouse, L. Z. Wu, C. H. Tung, T. R. Zhang, *Adv. Mater.* **2017**, *29*, 1605148.
- [91] D. Zhao, C. Dong, B. Wang, C. Chen, Y. C. Huang, Z. D. Diao, S. Z. Li, L. J. Guo, S. H. Shen, *Adv. Mater.* **2019**, 1903545.
- [92] M. A. Rahman, J. P. Thomas, K. T. Leung, *Adv. Energy Mater.* **2017**, *8*, 1701234.
- [93] H. N. Shi, S. R. Long, S. Hu, J. G. Hou, W. J. Ni, C. S. Song, K. Y. Li, G. G. Gurzadyan, X. W. Guo, *Appl. Catal., B* **2019**, *245*, 760.
- [94] J. Y. Zheng, Y. H. Lyu, C. Xie, R. L. Wang, L. Tao, H. B. Wu, H. J. Zhou, S. P. Jiang, S. Y. Wang, *Adv. Mater.* **2018**, *30*, 1801773.
- [95] X. Q. Hao, Z. W. Cuia, J. Zhou, Y. C. Wang, Y. Hu, Y. Wang, Z. G. Zou, *Nano Energy* **2018**, *52*, 105.
- [96] G. G. Liu, G. X. Zhao, W. Zhou, Y. Y. Liu, H. Pang, H. B. Zhang, D. Hao, X. G. Meng, T. Kako, P. Li, J. H. Ye, *Adv. Funct. Mater.* **2016**, *26*, 6822.
- [97] H. Li, J. Shang, H. Zhu, Z. Yang, L. Zhang, *ACS Catal.* **2016**, *6*, 8276.
- [98] I. Shown, S. Samireddi, Y. C. Chang, R. Putikam, P. H. Chang, A. Sabbah, F. Y. Fu, W. F. Chen, C. I. Wu, T. Y. Yu, *Nat. Commun.* **2018**, *9*, 169.
- [99] L. Xinwei, Z. Wendong, L. Jieyuan, J. Guangming, Z. Ying, L. Shuncheng, D. Fan, *Appl. Catal., B* **2019**, *241*, 187.
- [100] G. Yin, X. Huang, T. Chen, Z. Wei, Q. Bi, X. Jing, Y. F. Han, F. Huang, *ACS Catal.* **2017**, *8*, 1009.
- [101] D. Wu, W. Wang, F. Tan, F. Sun, H. Lu, X. Qiao, *RSC Adv.* **2013**, *3*, 20054.
- [102] Y. Li, R. Jin, X. Yan, J. Li, R. Jin, *Adv. Energy Mater.* **2016**, *6*, 1601273.
- [103] P. Ren, M. Song, J. Lee, J. Zheng, D. Li, *Adv. Mater. Interfaces* **2019**, *6*, 1901121.
- [104] C. L. Huang, W. L. Weng, Y. S. Huang, C. N. Liao, *Nanoscale* **2019**, *29*, 13709.
- [105] W. Feng, Z. Fang, W. Bo, L. Zhang, Z. Yan, Y. Yu, M. Huang, S. Weng, L. Ping, *J. Mater. Chem. A* **2017**, *5*, 1387.
- [106] S. Barja, S. Refaelly-Abramson, B. Schuler, D. Y. Qiu, A. Pulkin, S. Wickenburg, H. Ryu, M. M. Ugeda, C. Kastl, C. Chen, C. Hwang, A. Schwartzberg, S. Aloni, S.-K. Mo, D. F. Ogletree, M. F. Crommie, O. V. Yazyev, S. G. Louie, J. B. Neaton, A. Weber-Bargioni, *Nat. Commun.* **2019**, *10*, 3382.
- [107] X. Zhang, Y. Zhao, R. Shi, G. I. N. Waterhouse, T. Zhang, *Adv. Energy Mater.* **2019**, *9*, 1900881.
- [108] W. Wang, H. Zhang, S. Zhang, Y. Liu, G. Wang, C. Sun, H. Zhao, *Angew. Chem., Int. Ed.* **2019**, <https://doi.org/10.1002/anie.201908640>.
- [109] H. Feng, Z. Xu, R. Long, L. Chen, S. X. Dou, *ACS Catal.* **2018**, *8*, 4288.
- [110] X. D. Li, Y. F. Sun, J. Q. Xu, Y. J. Shao, J. Wu, X. L. Xu, Y. Pan, H. X. Ju, J. F. Zhu, Y. Xie, *Nat. Energy* **2019**, *4*, 690.
- [111] J. Yang, Y. Guo, R. Jiang, F. Qin, H. Zhang, W. Lu, J. Wang, J. Yu, *J. Am. Chem. Soc.* **2018**, *140*, 8497.
- [112] a) J. Li, X. Wu, W. Pan, G. Zhang, H. Chen, *Angew. Chem., Int. Ed.* **2017**, *57*, 491; b) Y. Zhang, Z. Xu, G. Li, X. Huang, W. Hao, Y. Bi, *Angew. Chem., Int. Ed.* **2019**, *131*, 14367.
- [113] L. Min, Y. Zhang, X. Li, Y. Wang, D. Fan, L. Ye, S. Yu, H. Huang, *ACS Sustainable Chem. Eng.* **2018**, *6*, 2395.
- [114] X. Deng, R. Li, S. K. Wu, L. Wang, J. H. Hu, J. Ma, W. B. Jiang, N. Zhang, X. S. Zheng, C. Gao, L. J. Wang, Q. Zhang, J. F. Zhu, Y. J. Xiong, *J. Am. Chem. Soc.* **2019**, *141*, 10924.
- [115] J. T. Li, S. K. Cushing, P. Zheng, T. Senty, F. K. Meng, A. D. Bristow, A. Manivannan, N. Q. Wu, *J. Am. Chem. Soc.* **2014**, *136*, 8438.
- [116] Z. L. Tian, P. F. Zhang, P. Qin, D. Sun, S. N. Zhang, X. W. Guo, W. Zhao, D. Y. Zhao, F. Q. Huang, *Adv. Energy Mater.* **2019**, *1901287*.
- [117] B. B. Zhang, L. Wang, Y. J. Zhang, Y. P. Ding, Y. P. Bi, *Angew. Chem., Int. Ed.* **2018**, *57*, 2248.
- [118] T. W. Kim, Y. Ping, G. A. Galli, K. S. Choi, *Nat. Commun.* **2015**, *6*, 8769.
- [119] M. Ma, K. Zhang, P. Li, M. Sun Jung, M. J. Jeong, J. H. Park, *Angew. Chem., Int. Ed.* **2016**, *55*, 11819.
- [120] M. Kim, B. Lee, H. Ju, J. Y. Kim, J. Kim, S. W. Lee, *Adv. Mater.* **2019**, *31*, 1903316.
- [121] Y. M. Fu, F. R. Cao, F. L. Wu, Z. D. Diao, J. Chen, S. H. Shen, L. Li, *Adv. Funct. Mater.* **2018**, *28*, 1706785.
- [122] P. Zhang, J. J. Zhang, J. L. Gong, *Chem. Soc. Rev.* **2014**, *43*, 4395.
- [123] H. F. Lin, B. W. Sun, H. Wang, Q. Q. Ruan, Y. L. Geng, Y. Y. Li, J. K. Wu, W. J. Wang, J. Liu, X. Wang, *Small* **2019**, *15*, 1804115.

- [124] X. Y. Zhang, Z. Zhao, W. W. Zhang, G. Q. Zhang, D. Qu, X. Miao, S. R. Sun, Z. C. Sun, *Small* **2016**, *12*, 793.
- [125] L. Pan, S. B. Wang, W. B. Mi, J. J. Song, J. J. Zou, L. Wang, X. W. Zhang, *Nano Energy* **2014**, *9*, 71.
- [126] Y. C. Zhang, N. Afzal, L. Pan, X. W. Zhang, J. J. Zou, *Adv. Sci.* **2019**, *6*, 1900053.
- [127] J. Wu, X. Li, W. Shi, P. Ling, Y. Sun, X. Jiao, S. Gao, L. Liang, J. Xu, W. Yan, C. Wang, Y. Xie, *Angew. Chem., Int. Ed.* **2018**, *57*, 8719.
- [128] S. Chen, H. Wang, Z. Kang, S. Jin, X. Zhang, X. Zheng, Z. Qi, J. Zhu, B. Pan, Y. Xie, *Nat. Commun.* **2019**, *10*, 788.
- [129] J. Hou, S. Cao, Y. Wu, F. Liang, Y. Sun, Z. Lin, L. Sun, *Nano Energy* **2017**, *32*, 359.
- [130] J. Hou, S. Cao, Y. Wu, F. Liang, L. Ye, Z. Lin, L. Sun, *Nano Energy* **2016**, *30*, 59.
- [131] H. Li, J. Shang, Z. Ai, L. Zhang, *J. Am. Chem. Soc.* **2015**, *137*, 6393.
- [132] S. Wang, X. Hai, X. Ding, K. Chang, Y. Xiang, X. Meng, Z. Yang, H. Chen, J. Ye, *Adv. Mater.* **2017**, *29*, 1701774.
- [133] J. H. Yang, Y. Z. Guo, R. B. Jiang, F. Qin, H. Zhang, W. Z. Lu, J. F. Wang, J. C. Yu, *J. Am. Chem. Soc.* **2018**, *140*, 8497.
- [134] H. Hirakawa, M. Hashimoto, Y. Shiraishi, T. Hirai, *J. Am. Chem. Soc.* **2017**, *139*, 10929.
- [135] Y. Zhao, Y. Zhao, G. I. N. Waterhouse, L. Zheng, X. Cao, F. Teng, L. Z. Wu, C. H. Tung, D. O'Hare, T. Zhang, *Adv. Mater.* **2017**, *29*, 1703828.
- [136] a) X. Sun, X. Luo, X. Zhang, J. Xie, S. Jin, H. Wang, X.-S. Zheng, X. Wu, Y. Xie, *J. Am. Chem. Soc.* **2019**, *141*, 3797; b) Y. Mao, P. Wang, L. Li, Z. Chen, H. Wang, Y. Li, S. Zhan, *Angew. Chem., Int. Ed.* **2019**, <https://doi.org/10.1002/anie.20191400>; c) L. Guo, Q. Zhao, H. Shen, X. Han, K. Zhang, D. Wang, F. Fu, B. Xu, *Catal. Sci. Technol.* **2019**, *9*, 3193; d) J. Yang, S. Hu, Y. Fang, S. Hoang, L. Li, W. Yang, Z. Liang, J. Wu, J. Hu, W. Xiao, C. Pan, Z. Luo, J. Ding, L. Zhang, Y. Guo, *ACS Catal.* **2019**, *9*, 9751.
- [137] H. Shang, M. Li, H. Li, S. Huang, C. Mao, Z. Ai, L. Zhang, *Environ. Sci. Technol.* **2019**, *53*, 6444.
- [138] a) S. Yang, Z. Huang, P. Wu, Y. Li, X. Dong, C. Li, N. Zhu, X. Duan, D. D. Dionysiou, *Appl. Catal., B* **2020**, *260*, 118129; b) S. Fan, X. Li, M. Qin, J. Mu, L. Wang, G. Gan, X. Wang, A. Chen, *ACS Omega* **2019**, *4*, 4113; c) W. Huo, W. Xu, T. Cao, X. Liu, Y. Zhang, F. Dong, *Appl. Catal., B* **2019**, *254*, 206; d) J. Hu, H. He, X. Zhou, Z. Li, Q. Shen, W. Luo, A. Alsaedi, T. Hayat, Y. Zhou, Z. Zou, *Chem. Commun.* **2019**, *55*, 5635.
- [139] a) Y. Xu, H. Li, B. Sun, P. Qiao, L. Ren, G. Tian, B. Jiang, K. Pan, W. Zhou, *Chem. Eng. J.* **2020**, *379*, 122295; b) Z. Chen, T. Fan, M. Shao, X. Yu, Q. Wu, J. Li, W. Fang, X. Yi, *Appl. Catal., B* **2019**, *242*, 40; c) J. Yang, D. Zheng, X. Xiao, X. Wu, X. Zuo, J. Nan, *Chem. Eng. J.* **2019**, *373*, 935.
- [140] a) B. Wang, M. Zhang, X. Cui, Z. Wang, M. Rager, Y. Yang, Z. Zou, Z. Wang, Z. Lin, *Angew. Chem., Int. Ed.* **2019**, <https://doi.org/10.1002/anie.201910471>; b) V. Sharma, T. Das, P. Ilaiyaraaja, C. Sudakar, *Sol. Energy* **2019**, *191*, 400; c) S. Jung, J. Lee, U. Kim, H. Park, *Sol. RRL* **2019**, *1900420*; d) J. Wang, S. Cao, J. Yu, *Sol. RRL* **2019**, <https://doi.org/10.1002/solr.201900469>